Inductor Design for Eddy-Current activated Lockin-Thermography

Diploma Thesis

of José Antonio Giménez Murcia

carried out at

Institute of Polymer Testing and Polymeter Science (IKP)

Department of Nondestructive Testing (ZfP)

University of Stuttgart

Departamento de Ingeniería de materiales y fabricación

Universidad Politécnica de Cartagena

2005

Resumen

La continua aparición de nuevos materiales y la necesidad de que estos se encuentren en perfecto estado debido a la función que desempeñan, como por ejemplo los materiales de que se componen los aviones, de los cuales dependen la vida de personas, hacen necesario el desarrollo de sistemas no destructivos de inspección de materiales, como la termografía. El modo de funcionamiento de este ensayo no destructivo es la generación de ondas térmicas dentro de las muestras a ensayar mediante diversos métodos, calentando la superficie con lámparas halógenas (termografía óptica), introduciendo ultrasonidos en la muestra (termografía de ultrasonidos) o introduciendo campos magnéticos en la muestra (termografía de inducción).

En este proyecto es desarrollada la termografía de inducción, la cual consiste en la generación de ondas térmicas dentro de los materiales mediante la introducción en estos de campos magnéticos. Estos campos son generados por un inductor conectado a un oscilador, el cual consiste en un circuito eléctrico con cuatro condensadores en paralelo y dos inductores en serie. Uno de los inductores es regulable y su función es la de ajustar la inducción total del sistema y el otro es el inductor encargado de generar los campos magnéticos. Este último es el objeto de este estudio, ya que los resultados obtenidos en las pruebas y la homogeneidad del calor en las muestras dependen de la geometría del inductor y de la configuración del circuito del oscilador. Los inductores generan una frecuencia de inducción que también depende de la geometría de este.

En este proyecto son comparadas diferentes formas de inductores, tales como inductores planos e inductores cilíndricos con núcleo de aire (solenoides) y también es investigada la influencia de la frecuencia de inducción en la penetración de la ondas térmicas en metales y en fibra de carbono. Ensayos en diferentes tipos de defectos, tales como corrosión y fisuras en metales, influencia en la orientación de las muestras de fibra de carbono con respecto a la dirección de los campos magnéticos generados por el inductor también son investigados, a la vez que es hecha una comparación entre termografía óptica y termografía de inducción.

En una segunda parte es desarrollado un sistema de inducción consistente en un inductor conectado a un amplificador, el cual recibe dos señales que simulan las frecuencias de inducción y de excitación del anterior sistema. La potencia de estas señales es amplificada y es introducida en el inductor, cuya función es generar campos magnéticos que calienten el material a ensayar.

La función de ambos sistemas es el mismo y son englobadas en la termografía de inducción, con la diferencia de la mayor economía de los aparatos de los que consta el segundo sistema.

Abstract

The continuous appearance of new materials and the necessity of their condition monitoring due to the functions that they fulfil, for example in security relevant structures like in planes, made it necessary to develop non-destructive testing systems for fast and reliable inspections.

One example of such an NDT-method is lockin-thermography which works with generation of thermal waves inside the sample under inspection. These thermal waves can be produced in different ways like heating the surfaces of the sample with halogen lamps (**O**ptical-**L**ockin-**T**hermography), introducing ultrasound into the sample (**U**ltrasound-**L**ockin-**T**hermography) or by eddy currents induced into the sample (**I**nduction-**L**ockin-**T**hermography). In this study the Induction-Lockin-Thermography is in focus. This method generates thermal waves by eddy currents introduced by an induction coil, which is connected to an electrical oscillator. The geometrical design of the inductor is the objective of this study as the results of inspection with ILT highly depends on the eddy current frequency, which governs the eddy current penetration depth, and on the homogeneity of heat deposition in the sample.

In this study different shapes of inductors like flat coils and cylindrical air cored inductors (solenoids) are compared. The influence of the induction frequency on the depth range for defect detection in metals and in CFRP is another objective in this project. Inspections on several kinds of defects like corrosion and cracks in metals are performed at different induction frequencies. An investigation on the influence of the orientation of CFRP samples with respect to the direction of the magnetic field and a comparison between optical and Induction-Lockin-Thermography is done.

In the second part of this work a new induction heating system is presented. It consists of an inductor connected to an audio amplifier. The advantage of this new system is its low price and the possibility of adjusting the eddy current frequency from 10 to 500 kHz. The two induction heating systems are compared.

I thank Prof. Busse that I was able to use the Induction-Lockin-Thermography equipment and technology of the IKP for my diploma thesis and for the financial support of the IKP-ZfP.
I also thank Prof. Dr. José Conde del Teso at the University of Cartagena.
Thanks also go to my adviser Gernot Riegert for guiding and supporting me.

Table of Contents

List of Figures

List of Tables

List of Symbols

Symbol	Description	Unit
R	Radius	mm
R	Resistance	Ohm
X	Impedance	Ohm
f	Frequency	Hz
L	Inductivity	μH
C	Capacity	nF
B	Magnetic field	T
l	Length	mm
A	Area	mm^2
I	Amperage	A

Greek Symbols	Description	Unit
α	Thermal conductivity	mm^2/s
μ	Permeability	H/m
μ_0	Permeability constant	H/m
μ_r	Relative permeability	-
μ	Thermal diffusion length	mm
κ	Electrical conductivity	S/m
ϕ	Magnetic flux	
δ_s	Penetration depth	mm

1. Introduction

Due to new materials being used in aerospace applications the requirements for NDE are changing, the most important problems are [1]:

- Components to be inspected are accessible only from one side.
- Non-flat surfaces.
- Highly anisotropic materials with a low thermal conductivity.
- Compounds of different materials with varying thermal properties are in use
- The need to monitor large surfaces in a short time to reduce the inspection time.

Security plays an important role in industry, in automotive applications or in aeronautical industry. The necessity of a system to analyse the material in search of defects without destroying it, becomes more and more important. Thermography is such a NDE method - it is based on thermal waves generated in different ways. These waves come back to the surface and with a infrared camera all the images are collected to generate two images, phase and amplitude image. Due to the inhomogeneity in the material caused by defects, these two images can show defects, which are not visible at first.
The advantage of this kind of non destructive evaluation is that the materials can be analysed by reflection without the necessity of disassembling the machine which is to be inspected.
Thermography includes several kinds of evaluations, between them is the induction lockin thermography, which consists of an inductor that generate magnetic fields, which go into the materials to heat it up and to generate thermal waves in them.
The design and production of inductors is the objective of this thesis, as the geometry and several other parameters of the inductors influence its inductivity which in turn influences the resulting eddy current frequency.
Low eddy current frequencies result in higher penetration depth, the eddy currents penetrate more into the material and with that heat more material. The goal of the thesis is to design several inductors with different inductivities in order to find out how the inductivity affects the eddy current frequency and with that the depth range for defect detection at Induction-Lockin-Thermography. This depth range does not

depend only on the eddy current frequency, it also depends on the penetration depth, which is related to the lockin frequency and this penetration depth has more influence in the complete penetration of waves in the material. Nevertheless, the influence of this penetration also depends on the material of the sample and its conductivity.

The modification of the characteristics of the system in induction lockin thermography, as well as the geometry of the inductor are discussed.

Another way to obtain eddy currents is a system based on an amplifier, which receive the two frequencies, induction frequency and lockin frequency by means of a signal generator and a computer respectively. The system is not developed and in this study some tests with this setup are obtained and compared with the previous setup. The inductors in this case are connected in the output of the amplifier and a new kind of inductors are developed, the Helmholtz coil. This kind of inductor consists of two coils with radius R, separated by the same distance, R. In that case, the samples can be introduced between them and the problem of the long air cored inductors is solved.
Depending on the distance between the coils in this kind of inductors, the magnetic filed generated between them change. In this study will be calculated the distance to obtain the most homogeneous magnetic field.

2. Active Lockin Thermography methods

Infrared thermography (IRT) is used for defect detection in the subsurface of materials and is basically divided in active and passive thermography methods.

- ***Passive thermography*** does not use sample excitation - for that the inspected probes have to have an elevated temperature as compared to the ambient. With that, abnormal temperature difference of some spots within the sample could indicate a potential defect. These spots are called **'delta-T'** or **"hot spots"**. In most of the applications, passive thermography is rather qualitative, because its purpose is only to detect anomalies of the type go/no-go, but these applications are based on empirical rules applied by experienced personal.

- ***Active thermography:*** In active thermography methods the samples are thermally excited and the thermal response of the sample evaluated. Quantitative characterization is possible by means of defect depth and approximate size.

  Active thermography includes several kinds of thermal stimulation: pulsed thermography, step-heating, lockin thermography. Another way of classification of active thermography methods is by its excitation devices like optical, vibrothermal, or inductive.

  - *Pulsed thermography (PT).* At pulsed thermography heat is applied in a short pulse and afterwards the temperature decay curve is recorded by an infrared camera. With the initial thermal pulse, the temperature of the material changes, due to a thermal front propagating by heat diffusion. The presence of a defect reduces the diffusion rate and with that this defect area has an increased temperature with respect to sound material. The deeper the defects within the sample the later their effect appears on the surface. They also have an reduced contrast due to the high damping of diffusion.

  The dependence of observation time (t) and thermal contrast (c) from the thermal diffusivity (α) and the defect depth (z) shows the following equation [2]:

$$t \approx \frac{z^2}{\alpha} \quad (2.1) \qquad c \approx \frac{1}{z^3} \quad (2.2)$$

  There is an empirical rule for PT: “The radius of the smallest detectable defect should be at least one or two times larger than its depth under the surface”. So, the defects that can be observed with PT will generally be shallow and the thermal contrasts will be weak.

  - *Step-heating (long pulse).* The increase in surface temperature is monitored by an infrared camera during the application of step heating (SH) pulse (“long pulse”). Variations of surface temperature with time are related to specimen features.

  This technique is used for applications such as coating thickness evaluation and there is an empirical relationship [3]:

$$t_c = \frac{0{,}36L^2}{\alpha} \qquad (2.3)$$

Where L is the coating thickness and α is the thermal diffusivity.
The specimen is heated and the temperature is plotted versus the square root of time and the thermal transit time is observed when the curve begins to depart from the semi-infinite case.

- *Lockin thermograhy (LT)*: There are several kinds of Lockin thermography but all are based on “thermal waves” which are generated inside the material in different ways. Lockin thermography is based on the analysis of thermal waves, which describe the temperature changes of a sample as a response to periodical or also to pulse excitation.

The thermal wave equation as a special solution of the heat diffusion equation is:

$$T(z,t) = T_0 \cdot e^{-\frac{z}{\mu}} \cdot e^{i\cdot(\omega t - \frac{z}{\mu})} \qquad (2.4)$$

The first part of this equation shows the damped amplitude, the second part the phase shift.

The thermal waves can be generated optically with halogen lamps or with a laser (“Optical-Lockin-Thermography”), with elastical waves (“Ultrasound-Lockin-Thermography”) and with eddy currents (“Induction-Lockin-Thermography”). In all cases the sample is excited at a particular angular frequency (ω) (“Lockin-Frequency”) which leads to thermal waves which penetrate into the material. The depth that the wave can reach depends on the Lockin-Frequency. The lower the frequency the higher the depth range. An infrared camera records several periods of excitation then a “phase image” and an “amplitude image” are calculated by Fourier transformation of the thermograms recorded.

2.1 Lockin-Thermography: amplitude and phase images

Parallel to the sample excitation the infrared camera records temperature images with a certain frame rate (i.e. 50 Hz). Each image consists of 610 x 430 pixels which correspond to the number of detectors in the focal plane array. The number of images recorded depends on the frame rate and on the number of acquisition periods of the chosen lockin-frequency. For example, if the frame rate of the camera is 50 Hz (50 images/s) at a lockin-frequency of 0.1 Hz (T=10 s) with 3 acquisition periods, the total number of images is:

N° images= 50 x 10 x 3= 1500

After recording the images, the computer performs a Fourier transformation at each pixel of the temperature image stag (eq. 2.5).

$$F(\omega) = \int f(t) \cdot e^{i\omega t} dt = \sum_i f(t) \cdot e^{i \cdot \omega \cdot t} \qquad (2.5)$$

The result is an amplitude and a phase image. The amplitude image is calculated by:

$$A(\omega) = \sqrt{Re(F(\omega))^2 + Im(F(\omega))^2} \qquad (2.6)$$

The phase image by:

$$\varphi(\omega) = \arctan\left(\frac{\mathrm{Im}\, F(\omega)}{\mathrm{Re}\, F(\omega)}\right) \qquad (2.7)$$

Amplitude images highly depend on the local emissivity (ε) of the sample as they show the local thermal emission. By propagating into the sample the thermal wave is highly damped. The depth range is given by the “thermal diffusion length (μ)”, expressed by:

$$\mu = \sqrt{\frac{2 \cdot k}{\omega \cdot \rho \cdot c}} \qquad (2.8)$$

k is the thermal conductivity

ω is the modulation frequency (lockin-frequency)

ρ is the density

c is the specific heat

The thermal diffusion length is defined as the depth where the phase (φ) is shifted by φ=1 rad and the amplitude is damped by 1/e. For amplitude images the depth range for defect detection is about one thermal diffusion length. As the thermal diffusion length not only depends on material parameters but also on the lockin-frequency it is possible to calculate the depth range for defect detection (eq. 2.8). The lower the modulation frequency the higher the depth range.

Phase images (eq. 2.7) show the phase shift of reflected thermal waves with respect to the excitation. The thermal waves penetrate into the material and are reflected at thermal boundaries like delaminations or cracks. The wave returns back to the surface where it is detected by an infrared camera. If the depth of the defect increases also the time of the thermal wave to return to the surface increases which leads to a higher phase shift in the phase image. After Fourier transformation of the superposed wave field on the surface of the sample the runtime difference of the reflected thermal waves to the excitation is monitored in a phase image. The depth range for defect detection at phase images is about two times the thermal diffusion length (μ) [4]. Phase images have the big advantage that they are independent of artefacts such as inhomogeneous heating or non uniform emission coefficient.

2.2 Optical-Lockin-Thermography (OLT)

Optical-Lockin-Thermography uses modulated optical light sources like laser or halogen lamps for sample excitation [5]. The lamps are sinusoidal modulated at the lockin-frequency. The light is absorbed on the surface of the sample which produces a modulated temperature field. From the field propagates a nearly plane thermal wave from the surface into the material and is reflected back to the surface by thermal boundaries. An infrared camera then records the thermal wave field of the superposed reflected thermal waves and the initial excitation (Fig. 1). A Fourier transformation over all pixel of the temperature image sequence then provides an amplitude and a phase image.

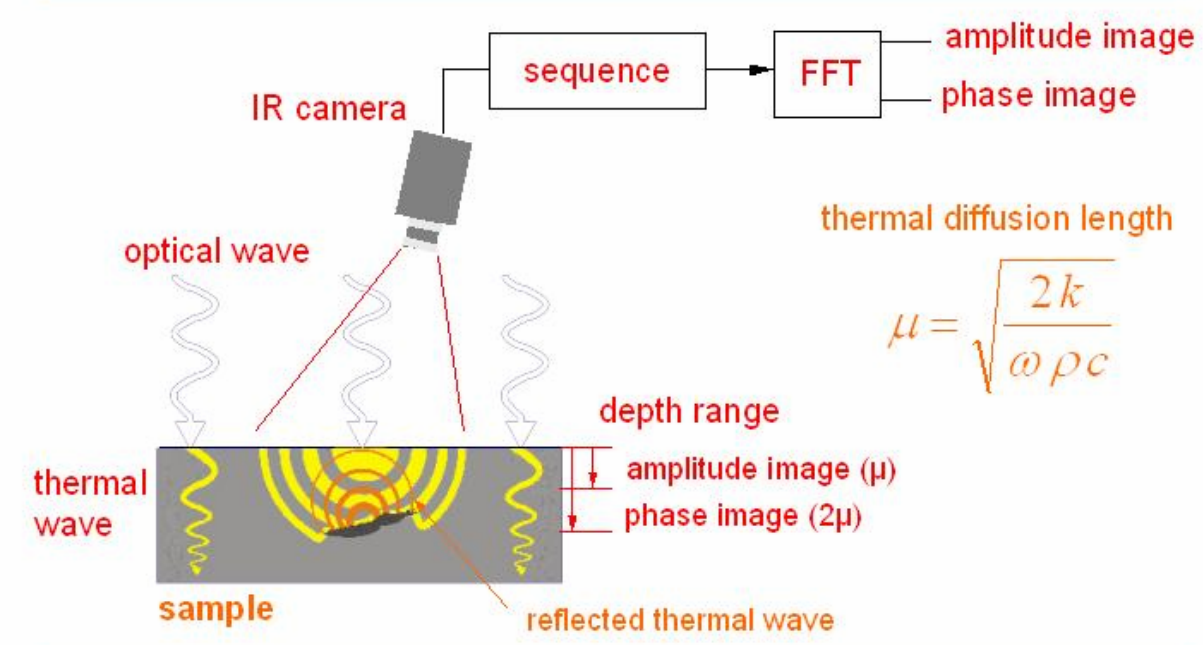

Figure 1: Optical-Lockin-Thermography schematical setup

2.3 Ultrasound-Lockin-Thermography (ULT)

Ultrasound thermography uses elastic waves for sample excitation. The setup consist of an piezoelectric transducer which is attached to the sample under inspection, a power amplifier, a unit control that is connected to a computer, and a thermography camera (Fig. 2).

The ultrasonic transducer launches amplitude modulated acoustic waves into the sample [6]. The modulated elastic waves propagate into the sample until they are converted into heat in high-loss-angle areas like defects. With that the defects are turned into generators of thermal waves which can be detected on the surface by an infrared camera. The temperature image sequence is Fourier analysed to provide a phase and an amplitude angle image.

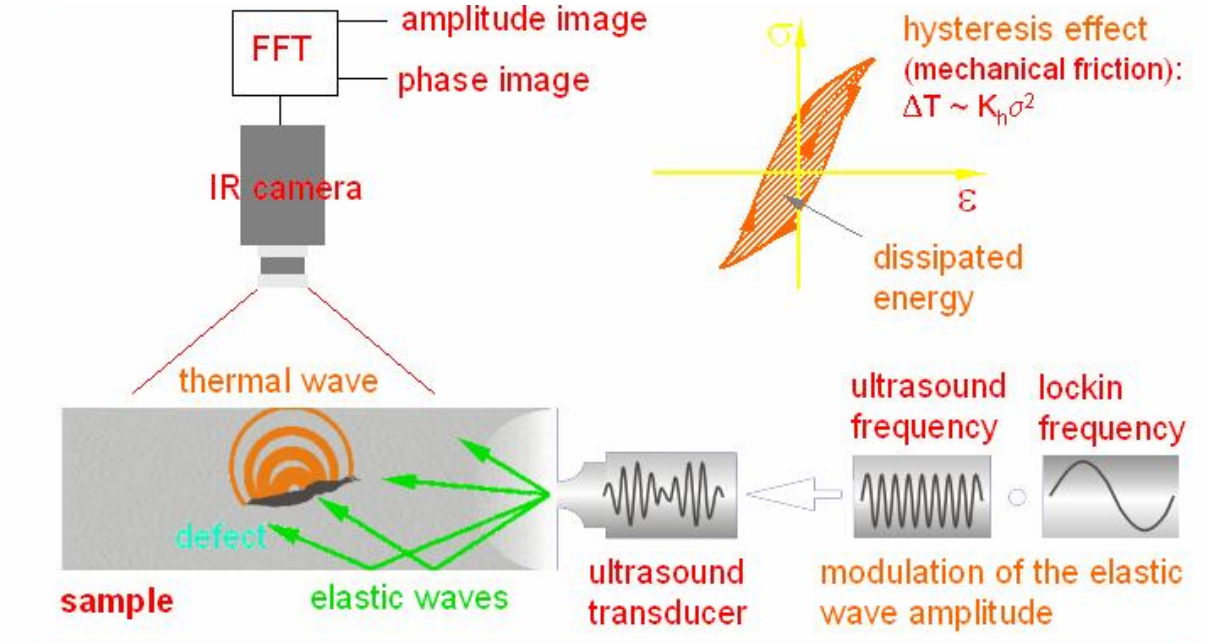

Figure 2: Ultrasound-Lockin-Thermography schematical setup.

The defect reveals itself by the internally generated and emitted thermal wave that is phase sensitively monitored when it arrives at the sample surface. So only the defect is detected and not the intact areas of the inspected component. The maximum depth range for defect detection is only noise limited and therefore basically larger than with optical excitation.

If a burst of ultrasound is used instead of an amplitude modulated signal, the Fourier transform provides images at various frequencies where higher frequencies display mainly near surface areas this is called Ultrasound Burst-Phase-Thermography (UBP) [7].

To avoid resonance frequencies and standing wave effects causing a pattern which might obscure real defects in the image, a frequency modulated ultrasound source operating at a centre frequency of about 20 kHz is used [8].

In some cases several transducers are attached to the sample which helps to reduce locally injected elastic wave power and to obtain more homogeneity in the noise of the phase angle.

2.4 Induction-Lockin-Thermography (ILT)

The idea of Induction-Lockin-Thermography is that a contact free induction coil induces eddy currents in conducting materials where the involved resistive losses are used for heating [9]. Similar to Ultrasound-Lockin-Thermography also the induction frequency is amplitude modulated. One measurement includes several modulation periods while an infrared camera records a temperature image sequence. A Fourier transformation provides an amplitude image and a phase image. Also at eddy current activated thermography the superiority of the lockin technique can be used. Especially the use of phase images in the Eddy current lockin thermography is of advantage, because it has a significantly better signal to noise ratio. As compared to single temperature shots and with the additional advantage that temperature gradients caused by inductive heating are eliminated.

The experimental setup of eddy current thermography consists of a generator with a maximum electrical output power of 1.5 kW (the output power is adjustable with an analogue interface which allows for amplitude modulation of the inductor power), an oscillator with a water-cooled inductor and a heat-exchanging device. The oscillator circuit is connected to the generator and this one and the infrared camera are connected to the computer (Fig. 3).

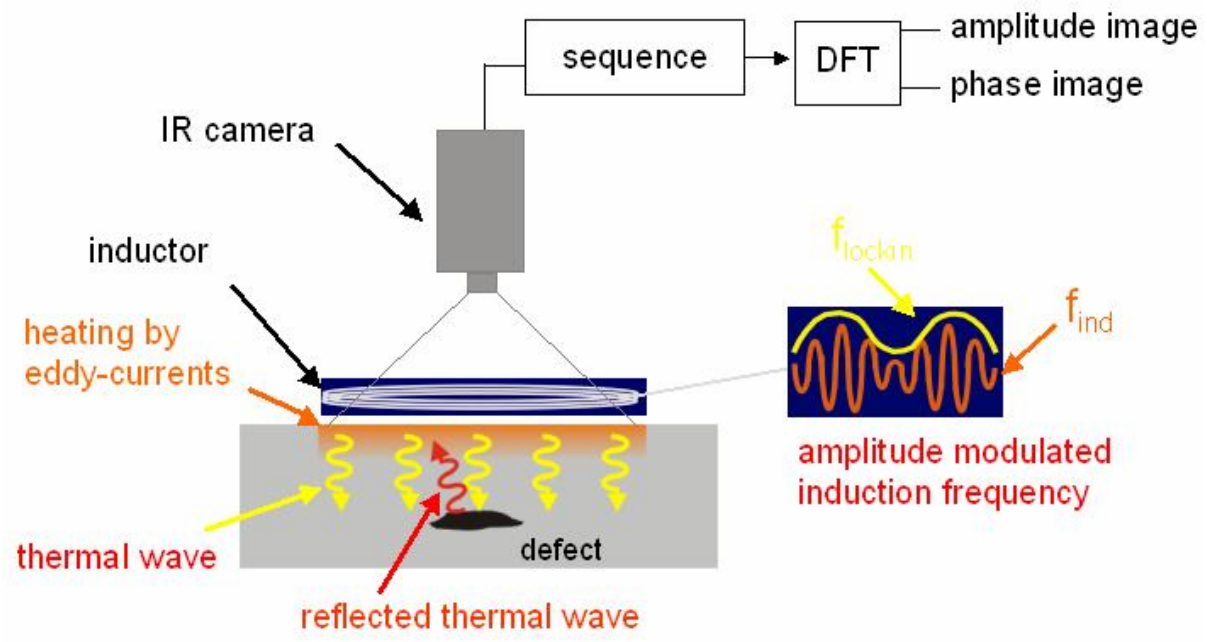

Figure 3: Induction-Lockin-Thermography schematical setup

Non destructive inspection with Induction-Lockin-Thermography is not limited to metallic materials as the sample only needs to have a minimum electrical conductivity.

3. Experimental setup

The Induction-Lockin-Thermography setup (Fig. 4) uses magnetic fields to heat up samples and an infrared camera for defect detection under the surface. This setup consists of several devices: generator, oscillator, heat exchanger, computer and infrared camera.

- Generator. It is connected to the oscillator and the computer. The generator supplies a maximun electrical power of 1,5 kW to the oscillator with the induction coil for sample heating. The maximum output voltage of the generator is 440 V and the eddy current frequency, which depends on the inductor connected to the oscillator, has a range from 30 kHz to 300 kHz.

- Oscillator. It is connected to the generator and the heat exchanger. The oscillator consists of a circuit, which is connected to the generator. The circuit consists of up to 4 parallel capacitors. Depending on their capacity, the eddy current frequency varies, the higher the capacity the lower is the frequency (section 5.3).
  In the circuit there is also a precoil, which ranges from 0 μH to 0,9 μH and can be adjusted in order to obtain the final desired eddy current frequency.

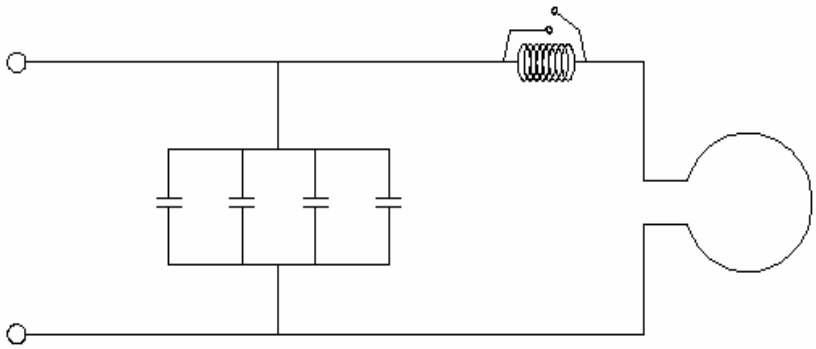

Figure 4: Oscillator circuit

The influence of this inductivity on the frequency is similar to the capacitor influence: when the inductivity increases, the frequency decreases.

The induction coil is also connected to the oscillator, and it produces magnetic fields, which heat up the sample to obtain with the infrared camera the neccesary images (phase and amplitude image, section 2.1 and 2.2) to see defects in the subsurface.

The frequency of this inductor is between 30 kHz and 300 kHz depending on its geometry and the depth, which can be reached depends also on this frequency (section 4.4).

- Heat exchanger. It is connected to the oscillator and also impels water into the induction coil to avoid excessive temperature increase.

- Infrared camera. It is connected to the computer and records temperature images simultaneously to the exctation.

- Computer. It is connected to the infrared camera and the generator. The computer controls the lockin frequency for excitation and therefore the thermal diffusion length (section 4.4). The condition periods in the test can also be adjusted which influences the measurement duration.

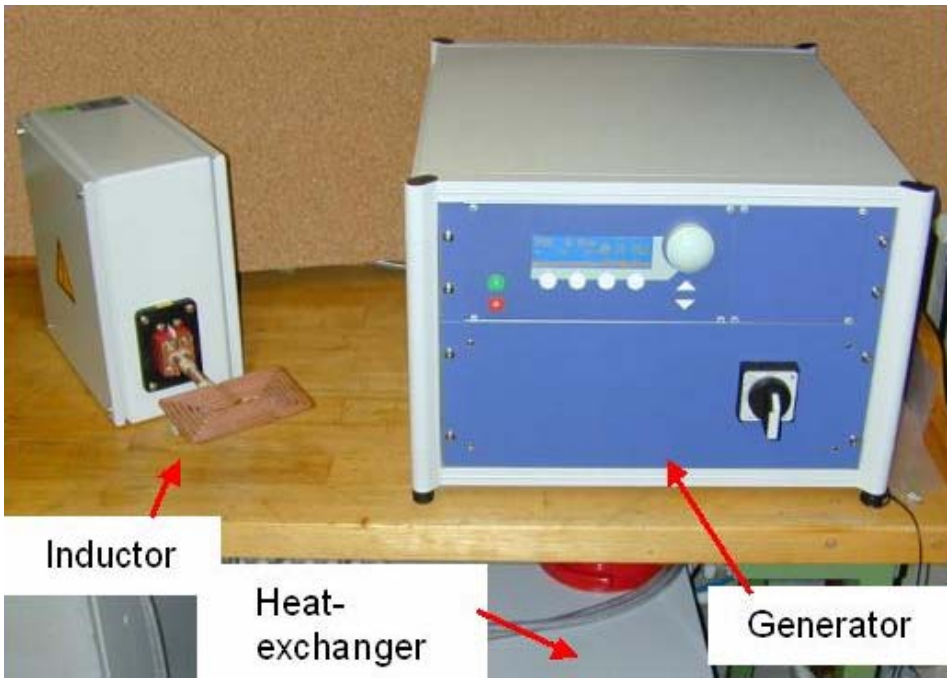

Figure 5: Induction-Lockin-Thermography experimental setup

4. ILT – depth ranges

There are two frequencies which determine the depth range of Induction-Lockin-Thermography: the eddy current frequency and the lockin frequency.

4.1 Eddy current penetration depth

With the induction coil the eddy current frequency can be adjusted. The objective of this thesis is to design an inductor, which modifies the frequency with a high homogeneity of the induced eddy current flow. By changing the geometric parameters (radius, length and number of windings), the inductor also changes its inductance. The penetration depth (δ_s) of the eddy currents depends on the "induction angular frequency" ($\omega = 2\pi \cdot f$), the "relative permeability" (μ_r) and the "conductivity of the material" (κ). The relative permeability and the conductivity are specific for each material. In metals the penetration depth of eddy currents is low due to the skin effect. It can be calculated by the following formula:

$$\delta_s = \sqrt{\frac{2}{\omega \cdot \mu \cdot \kappa}} = \sqrt{\frac{2}{\omega \cdot \mu_r \cdot \mu_0 \cdot \kappa}} \qquad (4.1)$$

The induction frequency should be in between 30 KHz and 300 KHz as these are the supported frequencies of the generator. The permeability constant (μ_0) is equal to 1.257 x 10-6 H/m. For steel the relative permeability is about μ_r=500, the electrical conductivity $\kappa = 10^6 \, S/m$. The following table (Tab. 1) shows different penetration depths in steel depending on the induction frequency (Eq. 4.1).

Penetration depth δ_s (mm)	Induction angular frequency (ω)	Induction frequency (f) (Hz)	Conductivity (κ) (S/m)	Permeability μ_0 (H/m)	Relative permeability
0,16	125663,6	20000	1000000	1,25664E-06	500
0,13	188495,4	30000	1000000	1,25664E-06	500
0,11	251327,2	40000	1000000	1,25664E-06	500

0,10	314159	50000	1000000	1,25664E-06	500
0,09	376990,8	60000	1000000	1,25664E-06	500
0,09	439822,6	70000	1000000	1,25664E-06	500
0,08	502654,4	80000	1000000	1,25664E-06	500
0,08	565486,2	90000	1000000	1,25664E-06	500
0,07	628318	100000	1000000	1,25664E-06	500
0,07	691149,8	110000	1000000	1,25664E-06	500
0,06	753981,6	120000	1000000	1,25664E-06	500
0,06	816813,4	130000	1000000	1,25664E-06	500
0,06	879645,2	140000	1000000	1,25664E-06	500
0,06	942477	150000	1000000	1,25664E-06	500
0,06	1005308,8	160000	1000000	1,25664E-06	500
0,05	1068140,6	170000	1000000	1,25664E-06	500
0,05	1130972,4	180000	1000000	1,25664E-06	500
0,05	1193804,2	190000	1000000	1,25664E-06	500
0,05	1256636	200000	1000000	1,25664E-06	500

Table 1: Eddy current penetration depth for steel depending on the induction frequency

The penetration depth is higher for lower frequencies. The penetration depth for steel at 20 KHz is equal to 0,159 mm.

4.2 Thermal diffusion length

As the eddy currents are used for induction heating in a lockin-thermography system, The thermal diffusion length (μ) depends on the Lockin frequency, its formula is:

$$\mu = \sqrt{\frac{2\alpha}{\omega}} \qquad (4.2)$$

Where α is the thermal conductivity and ω=2πf the lock-in frequency (f : frequency of temperature modulation), with values typically between 0,01 Hz and 1Hz. In the following table (Tab. 2) several values for the thermal diffusion length depending on the lockin frequency are shown.

Thermal conductivity (α)	Modulation frequency (ω)	Lockin frequency (f) (Hz)	Thermal diffusion length (μ) (mm)
18,8	0,1	0,01	24,5
18,8	0,3	0,05	10,9
18,8	0,6	0,1	7,7
18,8	0,9	0,15	6,3
18,8	1,3	0,2	5,5
18,8	1,6	0,25	4,9
18,8	1,9	0,3	4,5
18,8	2,2	0,35	4,1
18,8	2,5	0,4	3,9
18,8	2,8	0,45	3,6
18,8	3,1	0,5	3,5
18,8	3,5	0,55	3,3
18,8	3,8	0,6	3,2
18,8	4,1	0,65	3,0
18,8	4,4	0,7	2,9
18,8	4,7	0,75	2,8
18,8	5,0	0,8	2,7
18,8	5,3	0,85	2,7
18,8	5,7	0,9	2,6
18,8	6,0	0,95	2,5
18,8	6,3	1	2,4

Table 2: Thermal diffusion length for steel depending on the Lockin-frequency

In the case of phase images the depth range for defect detection is about twice (exactly 1,8 times) the “thermal diffusion length” and with that much higher than the “eddy current penetration depth”. The depth range for defect detection with eddy current can de increased significantly by using eddy current lockin thermography.

5. Adaption of eddy current frequency

As the penetration of the eddy currents into the sample depends on the eddy current frequency it is important to adapt this frequency to the actual measurement tasks. With a lower frequency, the waves have a higher penetration into the material than at higher frequencies. So it is necessary to adapt this frequency according to the desired penetration depth. This can be done by changing the frequency of the oscillator circuit (Sec. 5.2) or by changing the inductivity of the induction coil (Sec. 5.3).

The inductivity and with that also the induction frequency of the induction coil are adjustable by the length, number of windings and by the diameter of the inductor. The other possibility is changing the capacity of the oscillator circuit: higher capacity leads to a lower frequency. In the oscillator there is also a pre-coil with three ports: if the inductivity of the pre-coil increases, the induction frequency decreases.

In the following the inductor design and a trade study of the different parameters which have an influence on the resulting induction frequency is presented.

5.1 Basic formulas for air-cored inductor calculation

The inductivity of an air-cored inductor is calculated by the following formula [10]. It depends directly on the magnetic flux (ϕ), the number of windings (N), and the amperage (I).

$$L = N\frac{\phi}{I} \qquad (5.1)$$

On the other hand, the flux depends on the magnetic field (B) and the area of the inductor (A)

$$\phi = B \cdot A \qquad (5.2)$$

The magnetic fields are produced by electric currents and in a solenoid the magnetic field is concentrated into a nearly uniform field in the centre of a long solenoid. The field outside is weak and divergent. The magnetic field depends on the magnetic permeability and the auxiliary magnetic field (H).

$$B = \mu \cdot H \qquad (5.3)$$

Permeability is often expressed in relative (μ_r), rather than in absolute, terms.

$$\mu_r = \frac{\mu}{\mu_0} \qquad (5.4)$$

Where μ_0 represents the permeability of free space (μ_0 = 1.257 x 10^{-6} H/m) and μ the permeability of the substance in question (also specified in henrys per meter).

The auxiliary magnetic field (H) comes from:

$$H = N \cdot \frac{I}{l} \qquad (5.5)$$

Where N is the number of windings, I the amperage and l the length of the inductor. With (5.5) into (5.3), a new expression for the magnetic field is obtained:

$$B = \mu \frac{N \cdot I}{l} \qquad (5.6)$$

With (5.6) into (5.2) a new expression for the magnetic flux is obtained:

$$\phi = \mu \cdot \frac{N \cdot I}{l} \cdot A \qquad (5.7)$$

If the magnetic flux formula (5.7) is introduced in the inductivity formula (5.1), a new expression for the inductivity is obtained:

$$L = \mu \frac{N^2 \cdot A}{l} \qquad (5.8)$$

With this formula of a solenoid the inductivity of a long coil can be calculated. If the cross-section of the coil is circular, with a radius r, (measured from the axis to the centre line of the conductor) the area A will be:

$$A = \pi \cdot \frac{D^2}{4} = \pi \cdot R^2 \qquad (5.9)$$

The inductance is now with (5.9) in (5.8):

$$L = \mu \frac{D^2 \pi \ N^2}{4l} = \mu \frac{R^2 \pi \ N^2}{l} \qquad (5.10)$$

If the coil is made shorter, the field inside is no longer uniform, and the inductance becomes a function of the ratio of length to radius. Equation (5.10) stands only for long cylindrical coils (l >> D).

5.2 Electrical oscillator for eddy current generation

The purpose of the inductor is to use it in a system for induction heating in combination with an infrared camera for material inspection. This oscillator consists of a maximum of 4 capacitors and 2 inductances where one of these is the induction coil. The capacitors are in parallel, the inductances are in series. As the capacitors are parallel, the capacities are added to obtain the total capacity. The total capacity as well as the total inductivity in the oscillator circuit has an impact on the resulting eddy current frequency. The generator has a frequency range from 30 kHz to 300 kHz.

One of the two inductances in the circuit is a pre-coil, which can be modified by four steps in order to adjust the needed inductance. The induction coil is added to the oscillator therefore its inductance adds to that of the pre-coil. The induction coil produces eddy currents in electrical conductive samples and heats them up by electrical losses. With an infrared camera the temperature change on the surface of the sample can be monitored. The eddy current frequency depends mainly on the inductivity (L) and the capacity (C). If the inductivity of the inductor is increased, then the frequency decreases:

$$f = \frac{1}{2\pi \sqrt{L_{ges} \cdot C_{ges}}} \qquad (5.11)$$

The capacity has the same impact on the electrical oscillator as the inductivity: if it is increased the frequency decreases.

In our induction heating system two capacitors with 660 nF and two capacitors with 330 nF each are available. By adding the different capacitors in the 4 possible places capacities from 330 nF to 1980 nF can be obtained.
The different values for the induction frequency depending on the capacity are shown in the following table (Tab. 3).

Windings: N	outer diameter: D [mm]	p- factor [mm]	Length: l [mm]	Inductivity: L [µH]	Over all capacity: C [F]	**Eddy current frequency: f [kHz]**
13	78	10	130	7,8E+00	3,3E-07	9,92E+01
13	78	10	130	7,8E+00	6,6E-07	7,01E+01
13	78	10	130	7,8E+00	9,9E-07	5,73E+01
13	78	10	130	7,8E+00	1,3E-06	4,96E+01
13	78	10	130	7,8E+00	1,7E-06	4,43E+01
13	78	10	130	7,8E+00	2,0E-06	4,05E+01

Table 3: Values of induction frequency depending on the capacity in oscillator

By keeping all other parameters constant and only changing the inductivity of the pre-coil, the induction frequency changes. The pre-coil inductivity can be adjusted from 0 to 0,9 µH, in steps of 0,3 µH, that leads to: 0, 0.3, 0.6 and 0,9 µH. The following table shows the change of the induction frequency depending on the value of the pre-coil (Tab. 4).

Windings: N	Outer diameter: D [mm]	p- factor [mm]	Length: l [mm]	Pre-coil inductivity [µH]	Inductivity: L [µH]	Over all capacity: C [nF]	**Eddy current frequency: f [kHz]**
13	78	10	130	0	7,8E+00	1,7E-06	4,43E+01
13	78	10	130	0,3	8,1E+00	1,7E-06	4,35E+01
13	78	10	130	0,6	8,4E+00	1,7E-06	4,27E+01
13	78	10	130	0,9	8,7E+00	1,7E-06	4,20E+01

Table 4: Values of induction frequency depending on the inductivity of the pre-coil.

5.3 Design of air cored inductor

Depending on the desired eddy current penetration depth the necessary eddy current frequency has to be chosen. The inductor can have several geometries to obtain the same inductivity and consequently the same eddy current frequency (figure 6). If the capacity in the oscillator circuit (Sec. 5.2) is high, the inductivity of the inductor can be lower to obtain the same eddy current frequency. With equation 5.11 the necessary inductivity at a given capacity for a desired induction frequency is calculated.

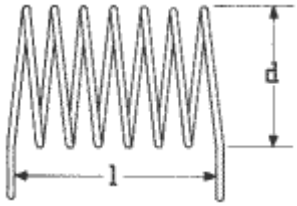

Figure 6: Geometry of an air cored inductor

As the inductivity (L) depends on several parameters like radius (r) or length (l) of the induction coil, the frequency depends also on them.

With equation 5.10 and the known inductivity, which has been obtained previously, the inductor parameters like number of windings, diameter and length (p-factor), are varied in order to get the most suitable geometry of the inductor. The p-factor is the distance between the windings, and therefore determines, together with N, the length of the inductor. In the following table several inductor parameters and their impact on the resulting eddy current frequency are shown (Tab. 5).

Number of windings: N	Outer diameter: D [mm]	P- factor [mm]	Length: l [mm]	Inductivity: L [µH]	Over all capacity: C [F]	Eddy current frequency: f [kHz]
1	78	10	10	6,0E-01	1,7E-06	1,60E+02
2	78	10	20	1,2E+00	1,7E-06	1,13E+02
3	78	10	30	1,8E+00	1,7E-06	9,23E+01
4	78	10	40	2,4E+00	1,7E-06	7,99E+01

5	78	10	50	3,0E+00	1,7E-06	7,15E+01
6	78	10	60	3,6E+00	1,7E-06	6,53E+01
7	78	10	70	4,2E+00	1,7E-06	6,04E+01
8	78	10	80	4,8E+00	1,7E-06	5,65E+01
9	78	10	90	5,4E+00	1,7E-06	5,33E+01
10	78	10	100	6,0E+00	1,7E-06	5,06E+01
11	78	10	110	6,6E+00	1,7E-06	4,82E+01
12	78	10	120	7,2E+00	1,7E-06	4,62E+01
13	78	10	130	7,8E+00	1,7E-06	4,43E+01
14	78	10	140	8,4E+00	1,7E-06	4,27E+01
15	78	10	150	9,0E+00	1,7E-06	4,13E+01
16	78	10	160	9,6E+00	1,7E-06	4,00E+01
17	78	10	170	1,0E+01	1,7E-06	3,88E+01
18	78	10	180	1,1E+01	1,7E-06	3,77E+01
19	78	10	190	1,1E+01	1,7E-06	3,67E+01
20	78	10	200	1,2E+01	1,7E-06	3,58E+01
21	78	10	210	1,3E+01	1,7E-06	3,49E+01
22	78	10	220	1,3E+01	1,7E-06	3,41E+01

Table 5: Eddy current frequency according to the geometry of the coil.

In this project an inductor with 13 windings, an outer diameter of 7,6 cm, a p-factor of 1 cm (length of 13 cm) and with a resulting eddy current frequency of 44,3 kHz was chosen.

5.4 Magnetic fields in electrical coils.

When a current carrying conductor is formed into a loop or several loops to form a coil, a magnetic field develops that flows through the centre of the loop or coil along the longitudinal axis and circles back around the outside of the loop or coil. The magnetic field circling each loop of wire combines with the fields from the other loops to produce a concentrated field down the centre of the coil. The magnetic field is essentially uniform down the length of the coil when it is wound more tightly.

The strength of a coil's magnetic field increases not only with increasing current but also with each loop that is added to the coil. A long straight coil of wire (“solenoid”) can be used to generate a nearly uniform magnetic field similar to that of a bar magnet. The magnetic field is concentrated inside of the coil.

5.4.1. Magnetic field generated by a single winding

To study the magnetic field in a inductor with several windings, it is necessary to study the magnetic field generated in a single winding.

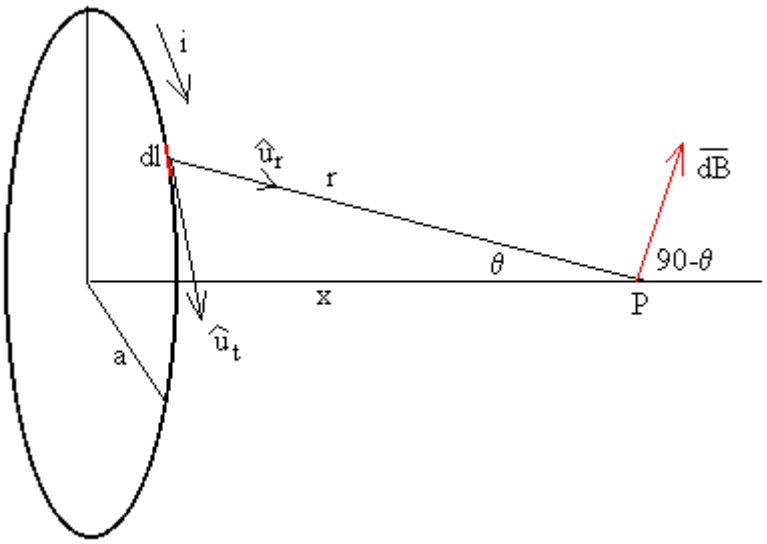

Figure 7: Magnetic field in a single winding.

Figure 7 shows a circular winding with radius a, and a current with intensity i travel around the winding. The point P is on the axis at a distance x from the centre of the winding.

If r is the distance between the current element and the point P, then the magnetic field generated by this current element can be calculated with the Biot-Savart law.

$$B(r) = \frac{\mu_0 I}{4\pi} \int_S \frac{ds' \times (r - r')}{|r - r'|^3} \qquad (5.12)$$

with the following vectors:

$$r = (0, 0, x), \quad r' = (a, 0, 0), \quad ds' = (0, a d\varphi', 0)$$

with that:

$$(r - r') = (-a, 0, x) \qquad (5.13)$$

and

$$|r - r'|^3 = \left(\sqrt{x^2 + a^2}\right)^3 \qquad (5.14)$$

and

$$[ds' \times (r-r')] = (a \times d\varphi', 0, a^2\, d\varphi') \qquad (5.15)$$

the field has only components on the z-axis out of symmetry reasons

With (5.14) and (5.15) in (5.12):

$$B_z = \frac{\mu_0 I}{4\pi} \int_0^{2\pi} \frac{a^2 d\varphi'}{\left(\sqrt{x^2 + a^2}\right)^3} = \frac{1}{2} \frac{\mu_0 \cdot I \cdot a^2}{\left(\sqrt{x^2 + a^2}\right)^3} \qquad (5.16)$$

This equation gives a relation of the magnetic field B in a point x on the axis of a single winding with radius a. In the centre of the winding (x = 0), the magnetic field is:

$$B = \frac{1}{2} \frac{\mu_0 \cdot I \cdot a^2}{\left(\sqrt{0 + a^2}\right)^3} = \frac{1}{2} \frac{\mu_0 \cdot I}{a^2} \qquad (5.17)$$

5.4.2. Magnetic field generated by several windings

The magnetic field generated by an inductor in one point (P), which is on the axis, is the addition of the magnetic fields generated by the N windings.

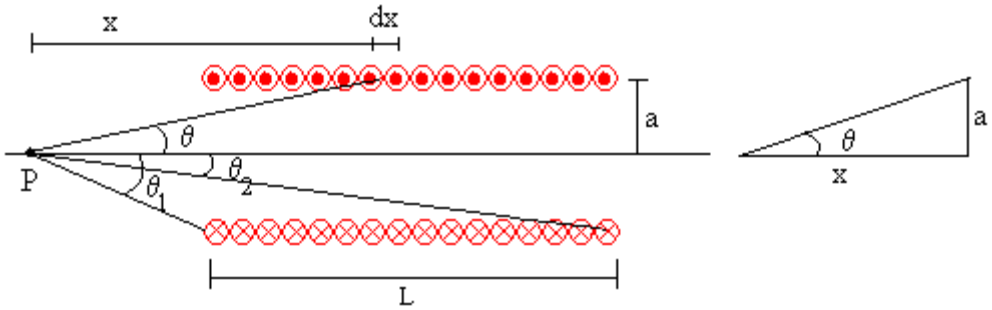

Figure 8: Magnetic field in a long coil of several windings

Figure 8 shows an inductor with length (L), which consists of N windings with radius (a). The windings generate in P a magnetic field, which has the same direction and the same way, it depends on the distance between x and P.

The number of windings between x and x+dx is dn=N·dx/L, these windings generate in P a magnetic field, which is the product of the magnetic field generated by one winding (eq. 5.16) multiplied by the number of windings dn.

$$dB = \frac{\mu_0 \cdot i \cdot a^2}{2\left(\sqrt{x^2 + a^2}\right)^3} \frac{N}{L} dx \qquad (5.18)$$

For integration, a variable substitution is done, a=x·tanθ, as $1+\tan^2\theta = 1/\cos^2\theta$, the integral is simplified.

$$1+\tan^2\theta = 1+\frac{\sin^2\theta}{\cos^2\theta} = 1+\frac{1-\cos^2\theta}{\cos^2\theta} = \frac{\cos^2\theta+1-\cos^2\theta}{\cos^2\theta} = \frac{1}{\cos^2\theta} \qquad (5.19)$$

The integral is

$$B = \frac{\mu_0 iN}{2L}\int_{\theta_1}^{\theta_2} -\sin\theta \cdot d\theta = \frac{\mu_0 iN}{2L}(\cos\theta_2 - \cos\theta_1) \qquad (5.20)$$

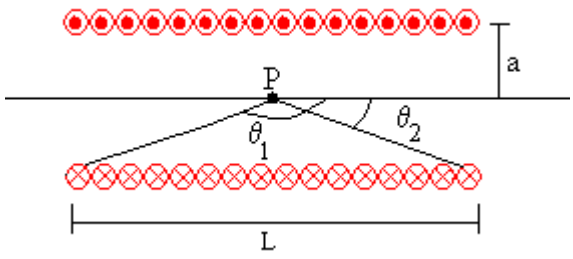

Figure 9: Magnetic field in a long coil: definition of angles

If the inductor is very long compared to its radius a and if the point P is located in centre, then $\theta_1 \to \pi$ and $\theta_2 \to 0$ (Fig. 9). The magnetic field value is now:

$$B = \frac{\mu_0 iN}{L} \qquad (5.21)$$

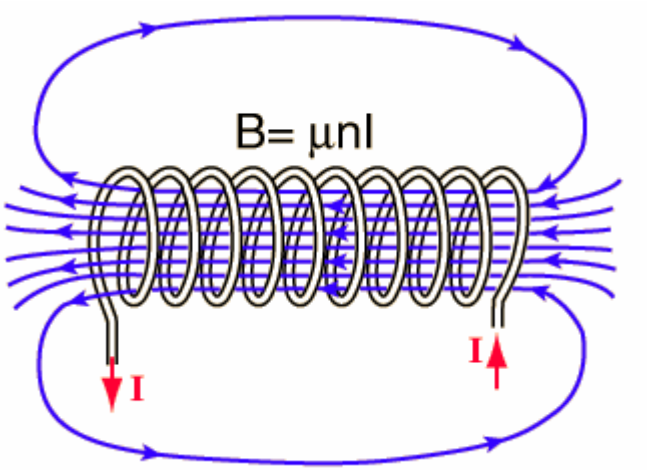

Figure 10: Magnetic field generated in an air cored inductor [11]

Figure 10 shows a schematical drawing of the magnetic field lines in a coil with several windings.

5.5 Inductivity measurement of produced induction coil

In the previous section the inductivity of a coil was calculated with several formulas which resulted in the desired geometry of the induction coil for the eddy current frequency needed (Tab. 6).

Number of windings: N	Outer diameter: D [mm]	P- factor [mm]	Length: l [mm]	Inductivity: L [μH]	Over all capacity: C [F]	Eddy current frequency: f [kHz]
13	78	10	130	7,8E+00	1,7E-06	4,43E+01

Table 6: Calculated properties of produced induction coil

The calculated inductivity of the produced coil is approximately 7,8 μH (Table 6). In order to check the actual inductivity of the coil the inductivity if it was measured with a gain-phase analyser (Fig. 11)

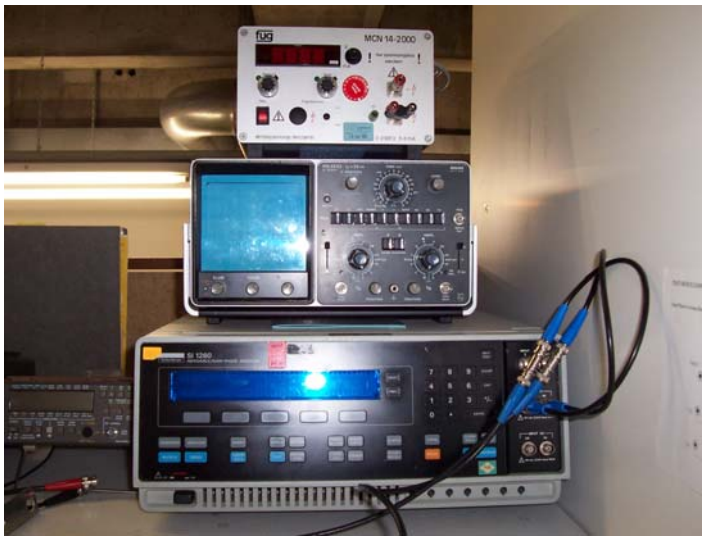

Figure 11: Impedance gain-phase analyser

This setup has a frequency range of 10 μHz to 32 MHz. It consists of a generator, which applies a drive signal and an analyser which correlates the input signals (V1, V2 and I) to the drive signal. The frequency can be sweeped within the frequency range in order to obtain the frequency response and impedance of the item under test.

The setup is connected to a computer, which records the data - in this case, the inductivity of the coil for several frequencies. With that is possible to see the behaviour of the inductivity with regard to the applied frequency.

As can be seen from equation (5.11), the inductivity of a coil decreases if the frequency increases. Table 7 shows the response of the produced coil on different input frequencies.

Frequency (Hz)	R (Ω)	X (Ω)	Z (Ω)	Inductivity (μH)	Angle
101530	0,33	4,91	4,92	7,69E+00	1,50
66986	0,31	3,25	3,26	7,72E+00	1,48
62500	0,31	3,03	3,05	7,72E+00	1,47
58315	0,31	2,83	2,85	7,72E+00	1,46
54409	0,31	2,64	2,66	7,72E+00	1,46
50766	0,30	2,46	2,48	7,73E+00	1,45

47366	0,30	2,30	2,32	7,73E+00	1,44
44194	0,30	2,15	2,17	7,73E+00	1,43
41235	0,30	2,00	2,03	7,74E+00	1,42
38473	0,30	1,87	1,89	7,74E+00	1,41
35897	0,30	1,75	1,77	7,75E+00	1,40

Table 7: Experimental results on induction coil

Table 7 shows the change of inductivity with the input frequency and the changes in resistance (R), complex resistance (X), and impedance (Z). The real part, resistance (R), does not depend on the input frequency and is approximately 0,3 Ω. The complex resistance (X) increases with the frequency. In this case there is no capacitance and therefore the imaginary part depends only on the inductivity of the coil (Figure 12).

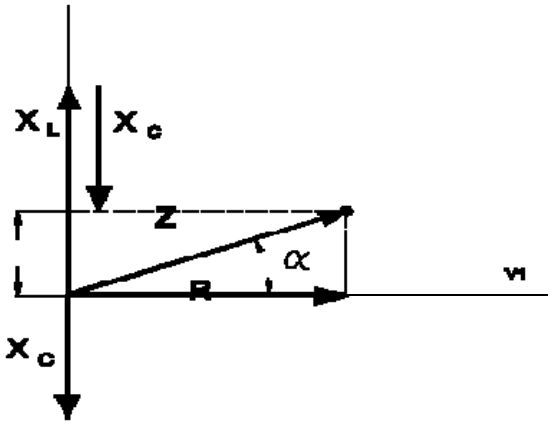

Figure 12: Relation of resistance (R), complex resistances (X_L, X_C) and impedance (Z) of a R-L-C oscillator

Figure 12 shows the impedance triangle for all possible cases of a R-L-C oscillator. In our case there is only inductivity, therefore the capacity has no influence on the imaginary part and on the angle. The following graphics show the change of the real and the imaginary part depending on frequency (Fig. 13).

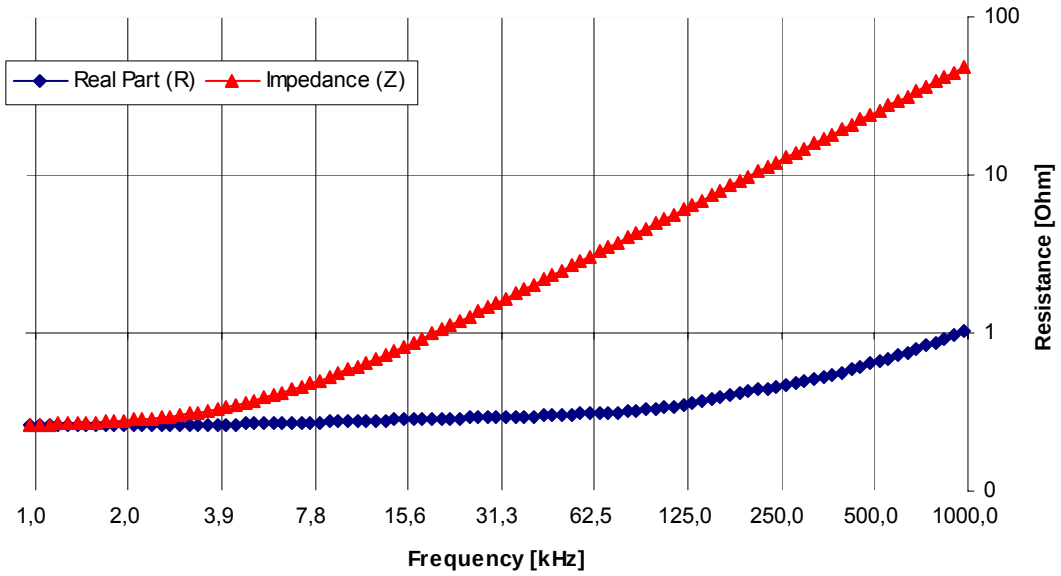

Figure 13: Dependency of Resistance and Impedance on input frequency

As it was expected, the resistance hardly changes and is practically constant as the resistance does not depend on frequency. The impedance increases with the input frequency.

6. Measurements and results

After the discussion about the inductivity of coils, some model samples are produced in order to show the improvements due to the coils depending on its geometry, eddy current frequency (which depends also on the inductivity of the coil and the capacity into the oscillator), and the orientation of the sample in the measurements. The first measurements are done on a steel plate with several slots, which have different depths, and on an CFRP tube with an impact damage of 50 J. Comparisons between images with different eddy current frequencies will be done in the following sections. Also the measurements with different orientations of the sample with regard to the coil and with different shapes of the coil will be compared.

6.1 Measurements on Metals

The inspected model sample is a plate of steel with several slots, which have different depths. The size of the sample is 222 x 160 x 8 mm and the remaining thicknesses of the slots are in depth order 0.3, 0.5, 0.7, 1, 1.2, 2, 3 and 4 mm.

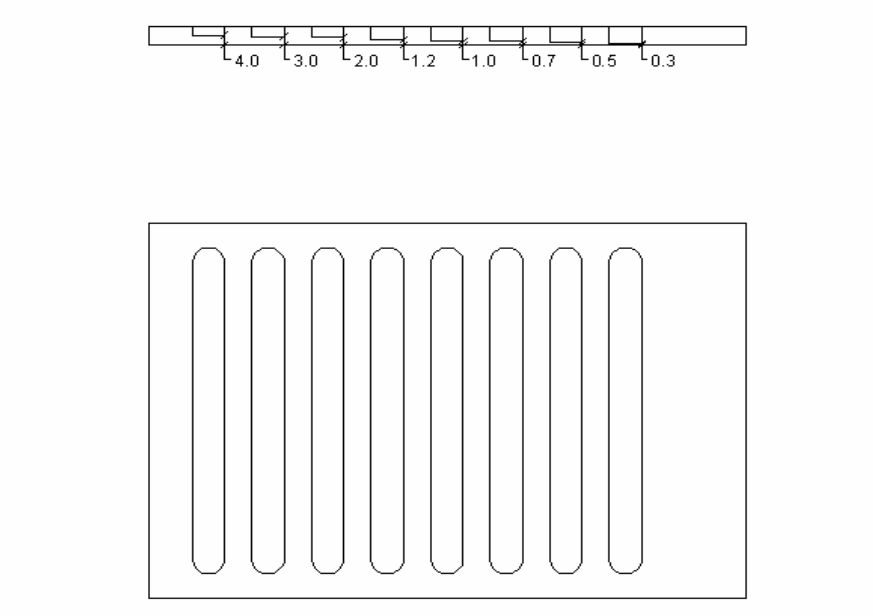

Figure 14: Sample for measurements in metals.

The following table shows the values for the thermal diffusion length depending on the lockin frequency.

Thermal conductivity (λ)	Modulation frequency (ω)	Lockin frequency (Hz)	Thermal diffusion length (μ) (mm)
18,8	1,88	0,3	4,46
18,8	3,14	0,5	3,45
18,8	6,28	1	2,44
18,8	9,42	1,5	1,99

Table 8: Thermal diffusion length for steel depending on the lockin frequency

The induction coil is in both cases the same, the change in the eddy current frequency is obtained by changing the capacitors in the oscillator (section 5.4). The induction frequencies, which are used to do the measurements, are 46 and 100 kHz. The position of the sample is the same in all measurements.

The waves generated by the induction coil have a defined lockin frequency which also determines the measurement duration as at least two periods should be recorded:

$$T = \frac{1}{f} \qquad (6.1)$$

In the following, there are several comparisons of measurements at the same lockin frequency but different induction frequencies.

Lockin frequency 1 Hz, electrical power 0.24 kW

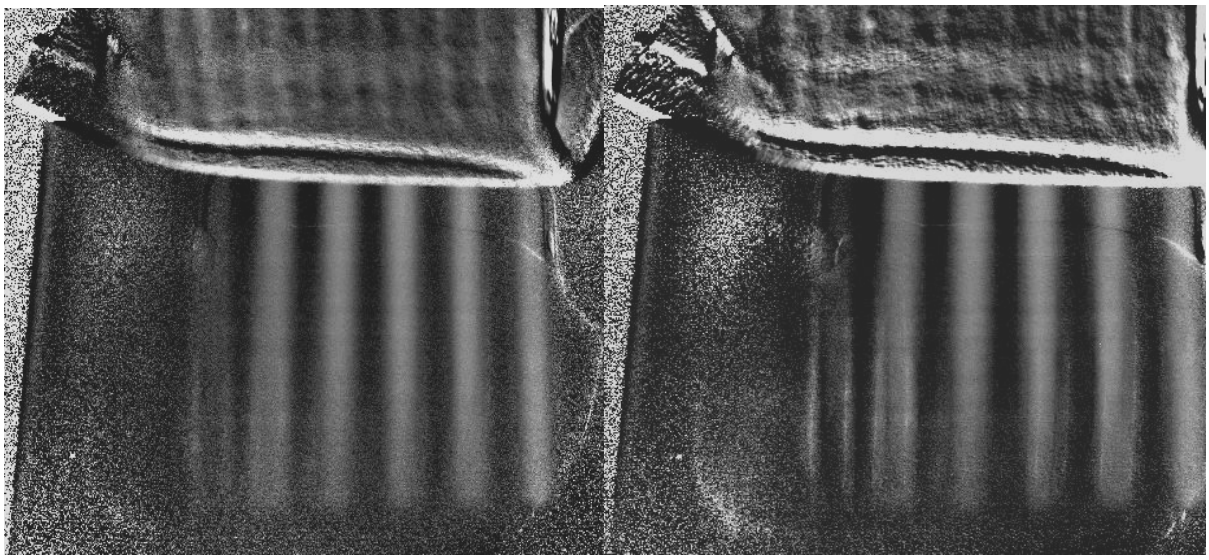

Figure 15: left: induction frequency 100 kHz, right: induction frequency 46 kHz

In these images the lockin frequency and the excitation power are the same. The position of the sample with regard to the inductor is the same in both measurements, the difference is only the induction frequency.

As the induction frequency differs also the penetration depth due to the different eddy current penetration depth should be different. In the previous images the induction frequencies are 100 and 46 kHz and the corresponding eddy current penetration depths are 0.07 and 0.1 mm respectively (table 9), so in the right image the waves reach a higher depth than in the left image, but the difference is too small to be detected.

Penetration depth δ_s (mm)	Induction-angular-frequency (ω)	Induction frequency (f) (kHz)	Conductivity (κ) (S/m)	Permeability μ_0 (H/m)	Relative permeability
0,10	314159	50	1000000	1,25664E-06	500
0,07	628318	100	1000000	1,25664E-06	500

Table 9: Values of penetration depth for 50 and 100 kHz.

The difference of remaining thickness in consecutive slots lies between 1 mm and 0.2 mm – with that the difference in the penetration depth of 0.03 mm cannot be resolved with this sample. This is why the results of both measurements are practically the same.

The followings images show the results of measurements with a lockin frequency of 1.5 Hz. The excitation amplitudes are different as 0.24 kW provided a poor signal noise ratio with an induction frequency of 46 kHz.

Lockin frequency 1.5 Hz

Electrical power 0.24 kW **Electrical power 0.48 kW**

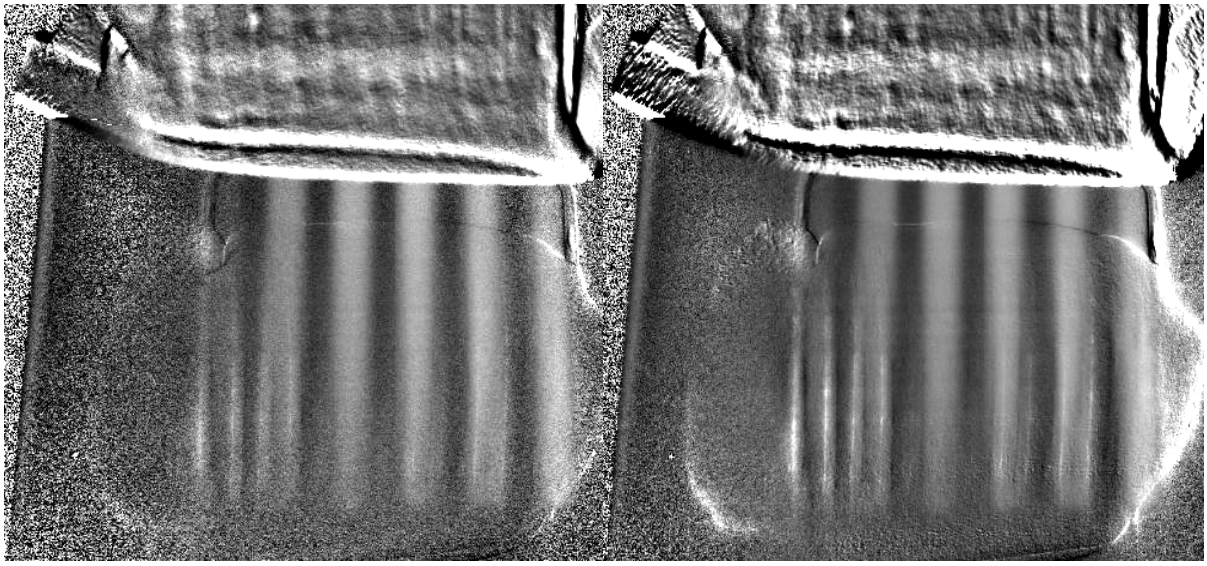

Figure 16: left: ind. frequency 100 kHz, right: ind. frequency 46 kHz

In the previous images, the lockin frequency is 1 Hz (Figure 15) and 1.5 Hz (Figure 16), the theoretical depth range for defect detection in phase images is approximately 4.4 mm and 3.6 mm respectively, and consequently all the slots should be visible – but are not. In the presented images there are two slots, which cannot be seen, their remaining thickness are 3 and 4 mm. The last slot on the left, which can be seen, has a remaining thickness of 2 mm and is not seen as well as the others. The reason for that is the lockin frequency of 1 and 1.5 Hz being too low – it should be higher. The problem is that the induction heating set up does not support frequencies much higher than that.

6.2 Measurements on metal sample with surface crack

The most common application of ILT is the detection of cracks in materials. In these measurements, the sample is a piece of metal with a thickness of 5 mm with three holes in the middle and a crack between the holes. The thermal diffusion length (section 4.2) in metal samples is:

Thermal conductivity (α)	Modulation frequency (ω)	Lockin frequency (f) (Hz)	Thermal diffusion length (μ) (mm)
18,8	6,28318	1	2,45
18,8	9,42477	1,5	1,99

Table 10: Thermal diffusion length in metals

In phases images the depth range for defect detection is 1.8 times the thermal diffusion length, so, for a lockin frequency of 1Hz and 1.5 Hz, is 4.41 and 3.6 mm respectively. The following images show some measurements of a metal crack sample with a lockin frequency of 1Hz. In this example the penetration depth is not of interest as the defect is directly on the surface.

Lockin frequency 1 Hz, electrical power 0.24 kW

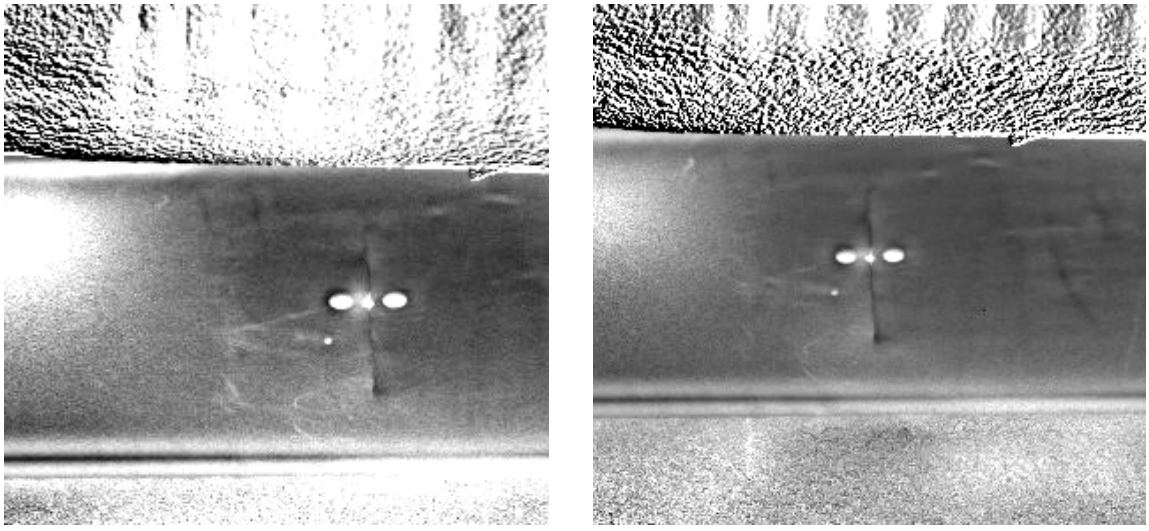

Figure 17: left: ind. frequency 100 kHz, right: ind. frequency 46 kHz

These images show measurements in the metal crack sample with a lockin frequency of 1 Hz, the homogeneity in the sample is very good and the boundaries of the crack are clearly seen. The difference between the two images is only the induc-

tion frequency, 100 kHz for the left image and 46 kHz for the right one. The penetration depth, which depends on the induction frequency, is 0.1 mm for 46 kHz and 0.07 mm for 100 kHz.

6.3 Corrosion under paint

In this section the possibility to use ILT to detect corrosion on metals under paint is analysed. The sample is a metal plate with intentionally added corrosion points under a non metallic coating.

The sample has a thickness of 1 mm, and a coating thickness of about 100 µm. In this case the lockin frequency is 1 Hz and consequently the thermal diffusion length is the same as in the images of the previous section, that is 4.41 mm. For this sample, the thermal diffusion length is not very relevant because the thickness of the sample is below the thermal diffusion length. The waves are generated in the metal under the paint and propagate through the layer to the surface.

Lockin frequency 1 Hz

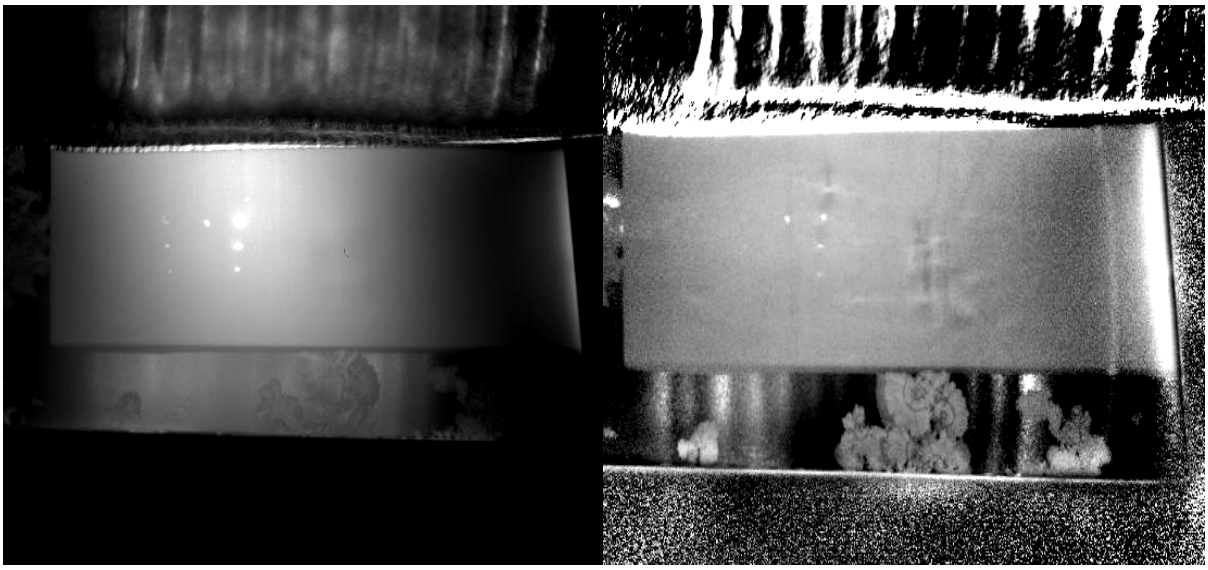

amplitude phase

Figure 18: Corrosion in metals

The left image shows the amplitude image, which shows the corrosion spots but also has a big gradient due to the inhomogeneous induction heating. The phase image on the right has a better homogeneity than the amplitude image although the defects have a higher contrast in the amplitude image. Nevertheless, also in the phase image it is possible to see the corrosion.

6.4 OLT compared to ILT.

In OLT the halogen lamps heat the surface of the sample and produce a thermal wave with the lockin frequency. In ILT the magnetic field penetrates into the sample and heat a material volume which depends on the penetration depth of the eddy currents - with that ILT should have a higher depth range than OLT due to the additional penetration depth of the eddy currents.
Concerning the homogeneity, in OLT the halogen lamps can heat a bigger sample than at ILT and the heat on the surface is more homogeneous. At ILT the size of the sample is important, because the magnetic field heats basically the zones next to the inductor, which results in a bad signal-to-noise ratio in other sample areas.
The sample which is used for the following measurements is the same as in section 6.1.

OLT, electrical power 0.72 kW ***ILT, electrical power 0.24 kW***

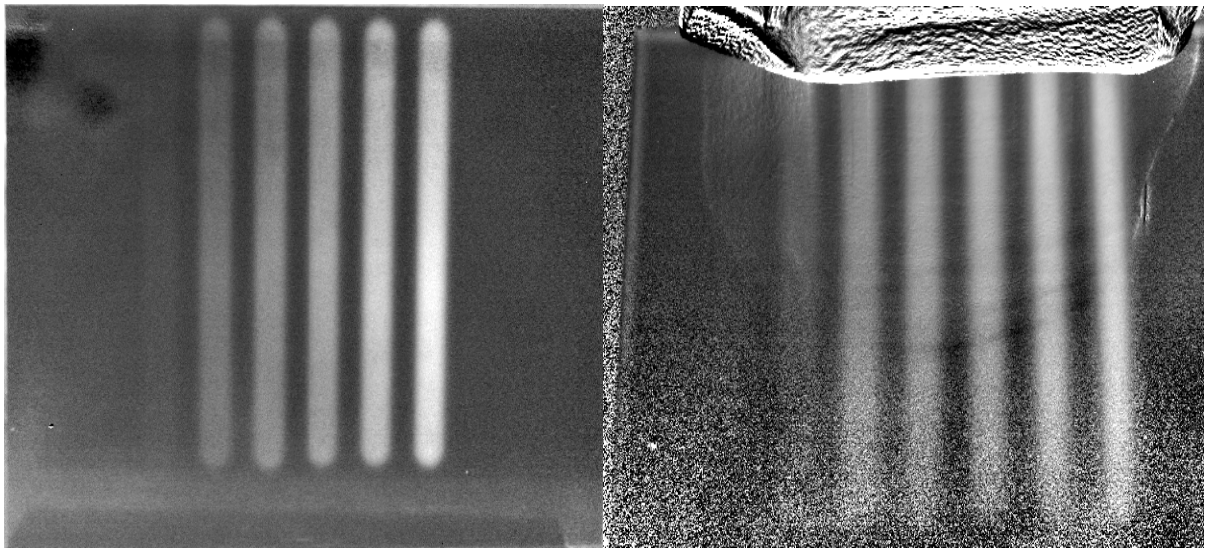

Figure 19: left: OLT Phase at 1.5 Hz, right: ILT Phase at 1.5 Hz

In these images the signal-to-noise in OLT is better than in ILT due to the more homogeneous heating. In ILT the signal-to-noise in the zones, which are far away from the inductor, is poor.
The lockin frequency is in both images 1.5 Hz. With this frequency the thermal diffusion length in ILT and OLT is approximately 3.6 mm and consequently, the last slot with a remaining thickness of 4 mm cannot be seen. The results in both images are very similar, but in the ILT image 6 slots can be clearly seen while in the OLT image only 5 are clearly visible.

6.5 Measurements on CFRP

For measurements in CFRP, the sample consists of a tube of CFRP with an impact of 50 J in the middle of its length.

Thermal conductivity (λ)	Modulation frequency (ω)	Lockin frequency (Hz)	Thermal diffusion length (μ) (mm)
0,4	1,884954	0,3	0,651470291
0,4	3,14159	0,5	0,504626718
0,4	5,026544	0,8	0,398942449
0,4	6,28318	1	0,356824974

Table 11: Values of thermal diffusion length for CFRP.

CFRP is a poor thermal conductor and consequently the thermal diffusion length is smaller than in metal samples. On the other hand the electrical conductivity is also poor – with that the eddy current penetration depth is high (up to 2 mm).

Lockin frequency 0.5 Hz

Electrical power 0.24 kW ***Electrical power 0.72 kW***

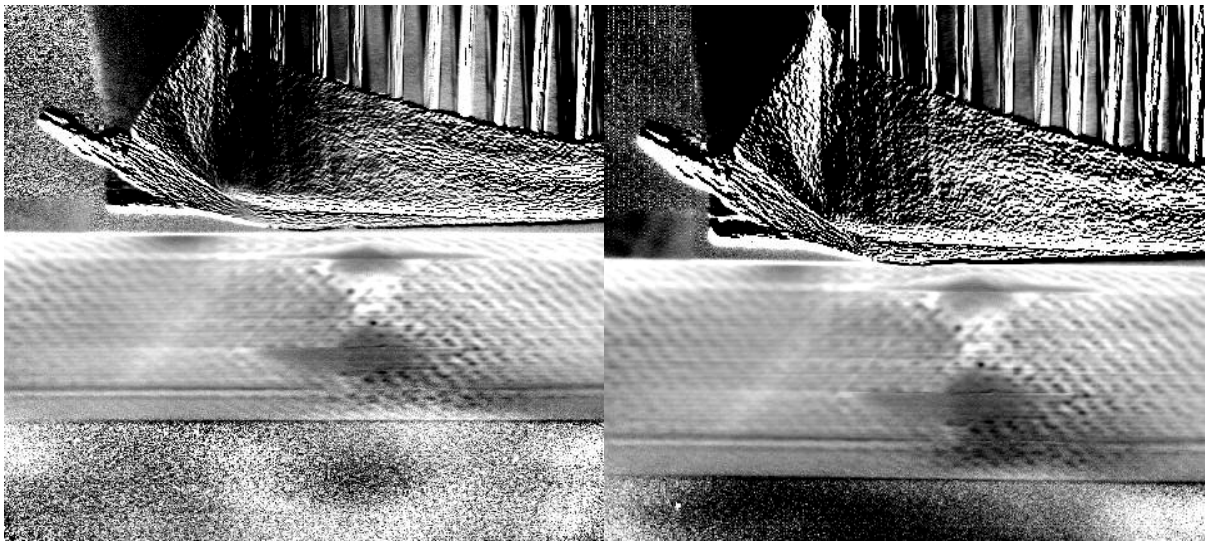

Figure 20: left: ind. frequency 100 kHz, right: ind. frequency 46 kHz

The previous images show the results of measurements on CFRP with a lockin frequency of 0.5 kHz. With this frequency, the thermal diffusion length is approximately 0.9 mm and the thickness of the tube is 1.3 mm. In the image on the right, an electrical power of 0.24 kW provides a poor signal to noise ratio, because the power is not

enough to heat all the sample and consequently an electrical power of 0.72 kW is used. All the parameters are the same in the two measurements except the induction frequency, but also in this case, the two images are very similar.

Lockin frequency 0.3 Hz

Electrical power 0.24 kW ***Electrical power 0.72 kW***

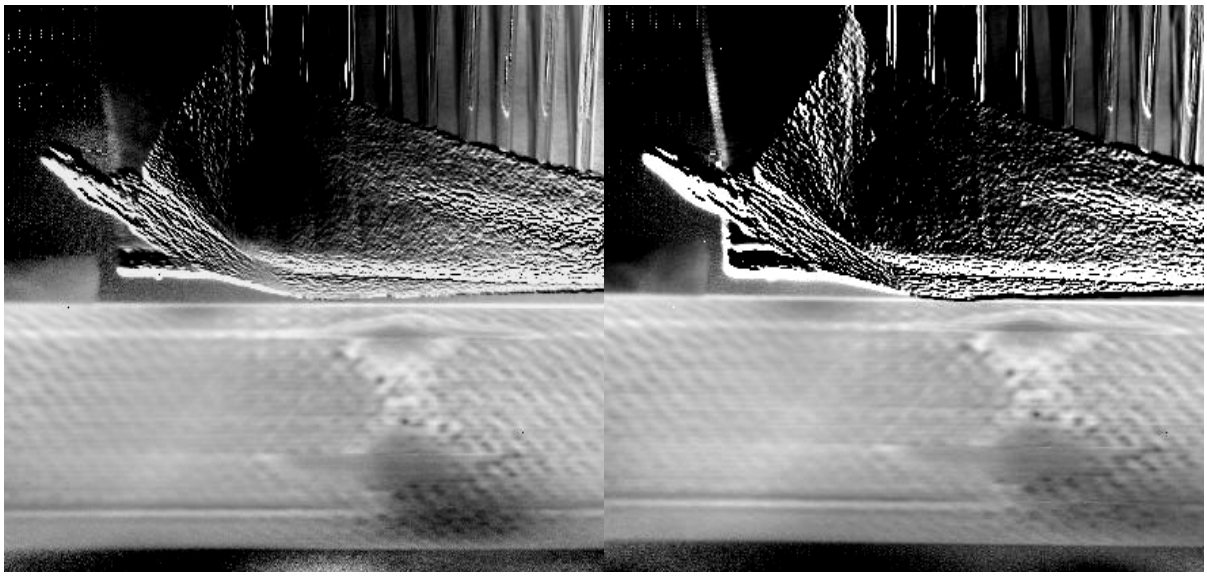

Figure 21: left: ind. frequency 100 kHz, right: 46 kHz

In these images, the lockin frequency is 0.3 Hz and with that lower than in the other images. With this frequency, the thermal diffusion length is approximately 1.3 mm, and the waves must penetrate more in the material than with 0.5 Hz of lockin frequency. These images are practically the same, because all the parameters are the same in the two measurements except the excitation power, and induction frequency. Here the difference in the penetration depth between the image with 46 kHz and the other with 100 kHz is also negligible, because the images do not show a big difference.

If the images at a lockin frequency of 0.5 Hz (Figure 20) are compared with the images at 0.3 Hz (Figure 21), there is a difference. In the first images, due to the lockin frequency (0.5 Hz) the waves penetrate less in the material than in the other images and theoretically the difference in the thermal diffusion length is 0.4 mm. So the first images (lockin frequency 0.5 Hz) show a more superficial image on the sample than in the last images, where the waves can penetrate deeper into the material.

6.6 Orientation dependency of ILT at CFRP

The results of measurements in CFRP samples depend on their orientation. CFRP consists out of electrical conductive carbon fibres and an epoxy matrix. Depending on the orientation of the fibres the interaction of the magnetic fields generated by the inductor (Figure 10) are influenced.

The following images show the results of several measurements on the rear side of a CFRP sample with an impact of 25 J.

Lockin frequency 0.3 Hz

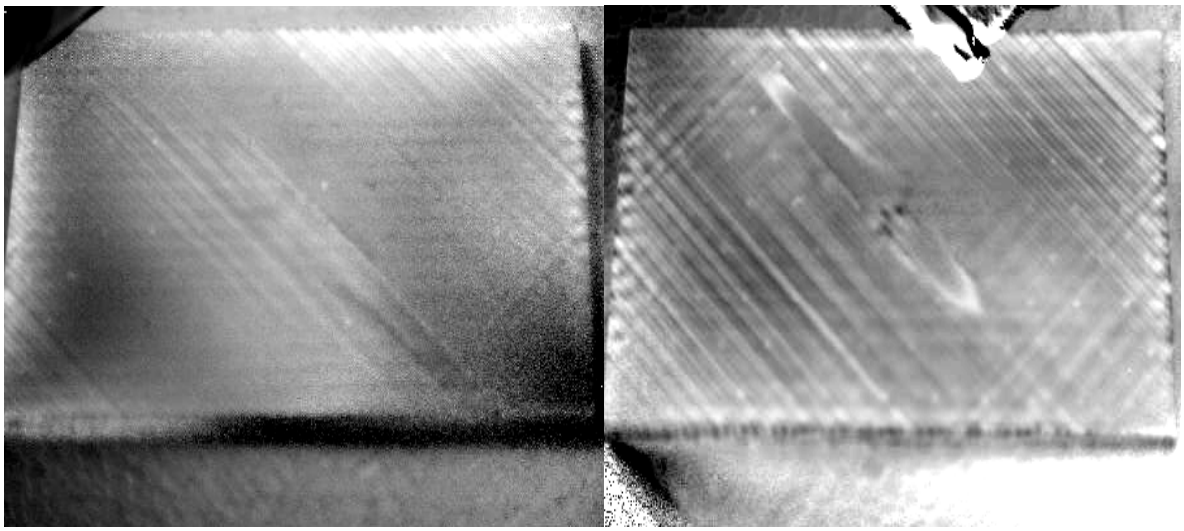

Figure 22: left: perpendicular orientation, right: parallel orientation

In the left image the orientation of the defect is perpendicular to the direction of the magnetic field, and in the right figure it is parallel. The lockin frequency is 0.3 Hz and the thermal diffusion length for this frequency is approximately 1.2 mm. The induction frequency is also the same for both images and equal to 46 kHz.

The images show that when the direction of the magnetic fields is parallel to the defect, it can be seen better than when it is perpendicular. In the first image the defect is not visible – the image only shows the orientation of the fibres in the sample. In the other image the outline of the defect is perfectly clear and the orientation of the fibres can also be seen.

Lockin frequency 0.5 Hz

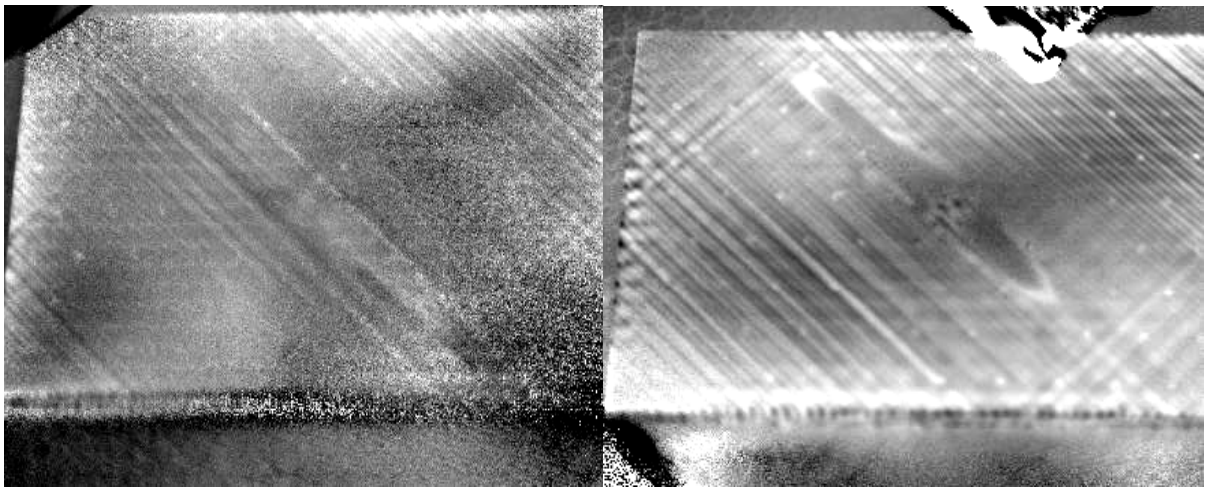

Figure 23: left: perpendicular orientation, right: parallel orientation

In these images the lockin frequency is 0.5 kHz and consequently the thermal diffusion length is approximately 0.9 mm. The induction frequency is the same in the two images and equal to 46 kHz. In this case, in the image in which the magnetic fields are perpendicular to the orientation (Fig. 23, left image) the defect is also not detectable like in the Fig. 22, left. In the other image (Fig. 23, right) in which the orientation of the defect is parallel to the magnetic field direction, the boundary of the defect is perfectly defined.

The difference between the images (with fibres parallel or perpendicular to the magnetic field) can be due to the fact that when the magnetic field hits the defect and if it is parallel, the magnetic field can excite the defect more efficiently and consequently the defect is better visible. In the other case, if the orientation of the fibres is perpendicular to the magnetic field the defects are not excited so the heat is not homogeneous and the impacts are not visible.

6.7 Impact of coil shape on results

In ILT, depending on the coil shape, the magnetic fields have a different distribution and consequently the homogeneity of the heat and the results are different when these are used in measurements. In this section, a flat coil and a long air cored inductor are used to get the images.

Lockin frequency 1 Hz, induction frequency 100 kHz

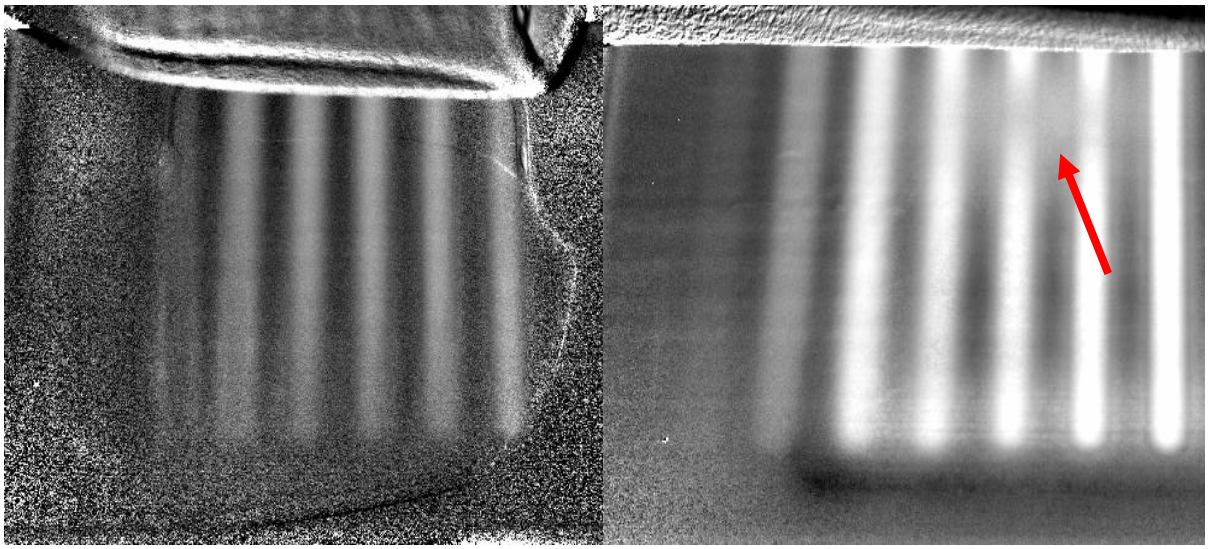

Figure 24: left: cylindrical coil, right: flat coil

The image on the left corresponds to an ILT measurement with a long air cored inductor, which is used in the previous sections, and the second image corresponds to an ILT measurement with a flat coil. The lockin frequency and the induction frequency are the same in both measurements: they are 1Hz and 100 kHz, respectively. Theoretically, the penetration depth and the thermal diffusion length are the same in both images and the waves reach the same depth, but due to the coil shape and the distribution of the magnetic fields in the sample and the homogeneity to heat it, the results are different.

In the first image (Fig. 24, left) the long air cored inductor shows an image with a not very good signal-to-noise because the outer field of the cylindrical coil is weak - 6 slots are seen in this test. At least the field in the area of the coil is homogeneous. The second image shows the same measurement, but with a flat coil. The signal-to-noise ratio is better due to a stronger magnetic field. In this image 6 slots are clearly seen and another one is hardly recognizable. But it also shows a blind spot which is due to the inhomogeneous field of the flat coil.

Lockin frequency 1.5 Hz, induction frequency 100 kHz

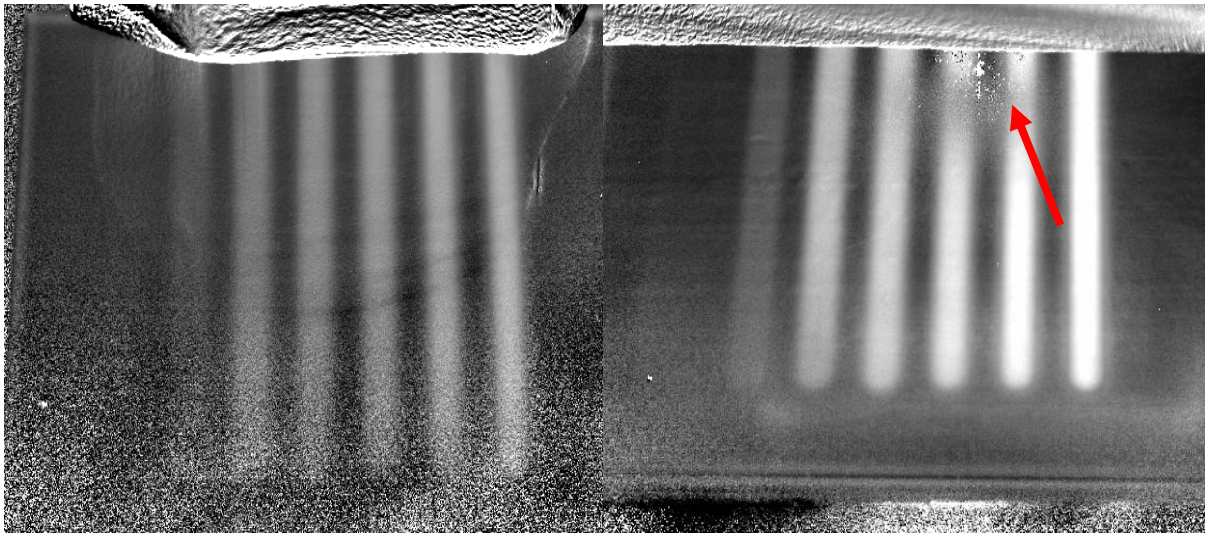

Figure 25: left: cylindrical coil, right: flat coil. Arrow indicates “blind spot” where low amplitude results in strong noise.

In this measurement the lockin frequency was changed and the induction frequency kept constant. The homogeneity and the signal-to-noise are very good in both images. With the air cored inductor 6 slots are seen and another one is hardly recognized, while with the flat coil the homogeneity is a little bit better and 6 slots are easily seen. The flat coil shows again the “blind spot” due to inhomogeneous heating.

7. Induction heating system with audio amplifier

7.1 Set-up of experiment

This new set-up tries to simulate the operation of the induction lockin thermography set-up. The operating system is different from the induction lockin thermography setup, but the result must be the same. The new set-up consists of a power amplifier, a signal generator, an infrared camera and a computer.

- Signal generator: This device generates the induction frequency - the maximum amplitude of the output must be less than 4V peak-to-peak, because this is the maximum input value of the power amplifier. The signal generator is connected to an oscilloscope to check the output power and afterwards connect to the power amplifier.

- Computer: The computer carries out the same function as in the other setup, that is, with the computer, the desired lockin frequency and amplitude are regulated, the signal goes into the signal generator and then from this, the two waves (induction frequency generated by the signal generator and the lockin frequency generated by the computer) go into the amplifier.

- Power amplifier: This device receives the two signals (induction frequency generated by the signal generator and lockin frequency generated by the computer) and it amplifies the amplitude. The output is connected to an induction coil, which carries out the same function as in the other setup: generate magnetic fields to heat up the sample.

- Infrared camera: Its function is exactly the same as in the other setup: it records a temperature image sequence which is analysed by the computer in order to calculate an amplitude and a phase image.

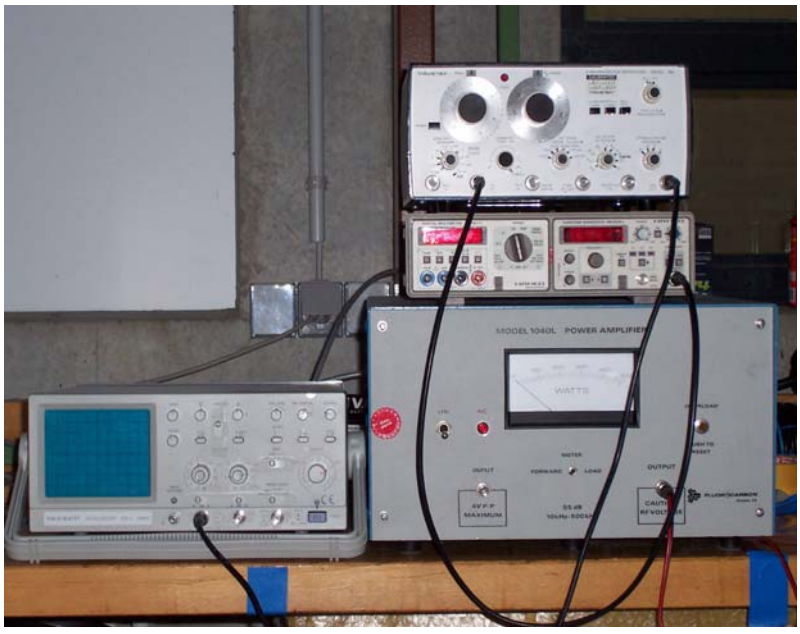

Figure 26: Induction heating system with audio amplifier.

7.2 Helmoltz coil design

The long coils practically excludes any possibility of access to the equipment inside. There is a way to solve this problem, the so called Helmholtz coils. This is a setup

that generates a homogenous field and allows access to the experimental area between the pair of coils. The setup consists of two circular identical coils located at a spacing exactly equal to their radius.

If it is considered that the magnetic field between the two coils has only “z” component and this component has the direction of the axis, which is perpendicular to the plane of the coils, using the Biot-Savart law it is possible to calculate the distance between the two coils to obtain the most homogeneous field between them.

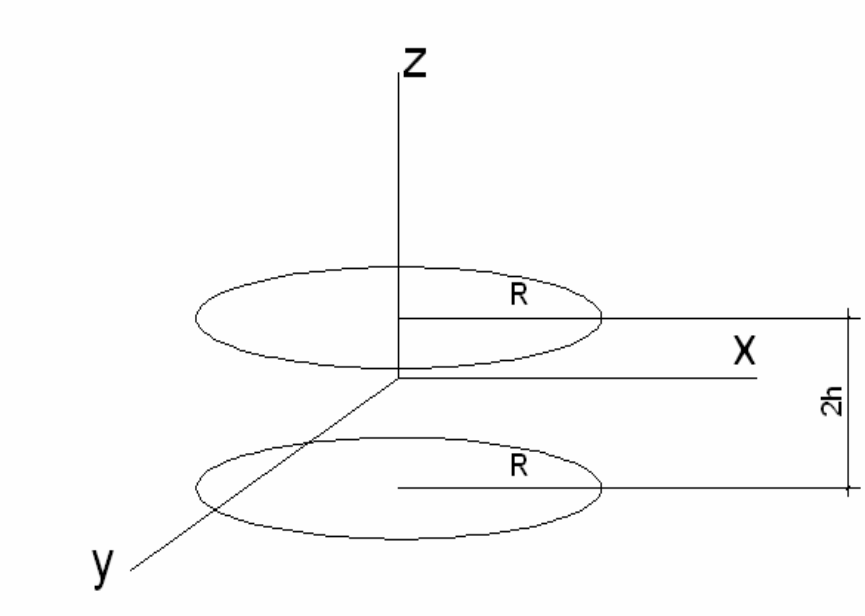

Figure 27: Helmholtz coil

If the Biot-Savart law is applied and only one direction of the magnetic field is considered (z axis), the magnetic field created by the coil with higher elevation in one point of the axis is (see also eq. 5.12 – 5.16):

$$B_z^1 = \frac{\mu_0 \cdot I \cdot R^2}{2 \cdot (R^2 + (z-h)^2)^{3/2}} \qquad (7.1)$$

The magnetic field generated by the other inductor is:

$$B_z^2 = \frac{\mu_0 \cdot I \cdot R^2}{2 \cdot (R^2 + (z+h)^2)^{3/2}} \qquad (7.2)$$

As μ_0 and R are constant:

$$K = \frac{\mu_0 \cdot R^2}{2} \quad \text{(constant)} \qquad (7.3)$$

The total magnetic field is the addition of both magnetic fields, and considering the constant (7.3), the total magnetic field is:

$$B_z(z) = K \cdot \left((R^2 + (z-h)^2)^{-3/2} + (R^2 + (z+h)^2)^{-3/2} \right) \qquad (7.4)$$

So the distance between the coils is 2h.
The first derivative of the total magnetic field is:

$$B_z^{'}(z) = -3K \cdot \left((z-h)(R^2 + (z-h)^2)^{-5/2} + (z+h)(R^2 + (z+h)^2)^{-5/2} \right) \qquad (7.5)$$

which is zero in the centre, as the symmetry of the problem demands.
The second derivative is:

$$B_z^{''}(z) = -3K \cdot \left((R^2 + (z-h)^2)^{-5/2} + (R^2 + (z+h)^2)^{-5/2} - 5 \cdot (z-h)^2 (R^2 + (z-h)^2)^{-7/2} - 5 \cdot (z+h)^2 (R^2 + (z+h)^2)^{-7/2} \right)$$

(7.6)

This equation in z=0 is:

$$B_z^{''}(0) = -3K \cdot (R^2 + h^2)^{-7/2} \left((R^2 + h^2) + (R^2 + h^2) - 5h^2 - 5h^2 \right) =$$

$$= -3K \cdot (R^2 + h^2)^{-7/2} \cdot (2R^2 - 8h^2) \qquad (7.7)$$

This equation is equal to zero (which means that the curvature of the field profile disappears) if:

$$h = \frac{R}{2} \qquad (7.8)$$

So in this Helmholtz arrangement with highest homogeneity the distance between the coils equals their radius.
With (7.8) in (7.1) the magnetic field along the axis at the midpoint between the two coils (z=0) is given by:

$$B = \frac{8\mu_0 I \cdot N}{5^{3/2} R} \qquad (7.9)$$

Where $\mu_0 = 4\pi \cdot 10^{-7}$ T•m/A, I is the current (A) in one coil, R is the radius of the coil and N is the number of turns of wire in one coil.
The distribution of the magnetic field in Helmholtz coils is shown in the following image.

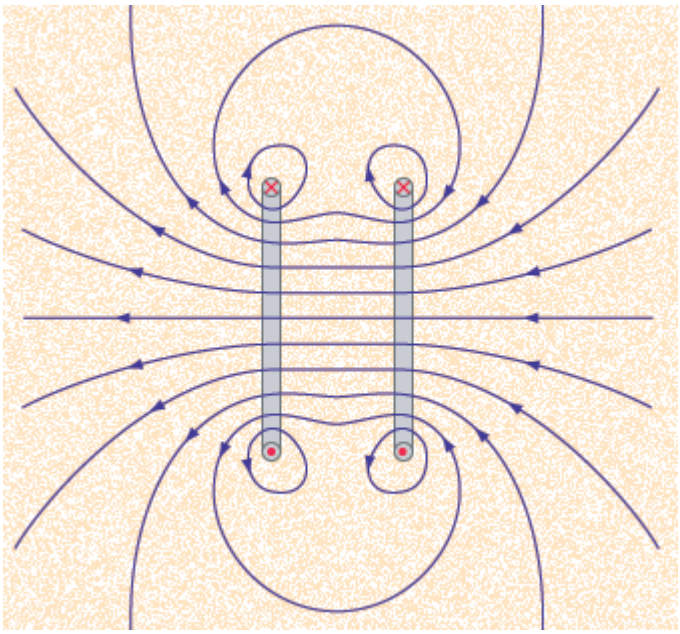

Figure 28: Magnetic field lines for Helmholtz coil

7.3 Measurements on metals

After the explanation of the new setup and the discussion about the homogeneity in Helmoltz coils, these are tested on a metal sample, which has already been used in section 6.2 and which consists of 3 holes with a crack perpendicular to the line that joins these holes. The Helmholtz coil consists of two coils of 4 windings each one separated a distance R, equal to the radius of the inductors.

Lockin frequency 1 Hz, induction frequency 400 kHz

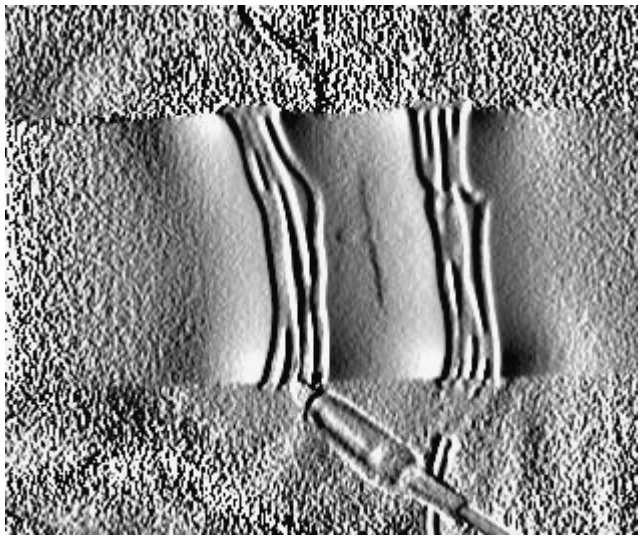

Figure 29: Test in metal sample with new setup.

The inductors are wound over the sample and the crack is in the middle of the distance, which separate the two inductors, precisely where the magnetic field is most homogeneous.

The lockin frequency in this measurement is 0.1 Hz and the thermal diffusion length in metals for this frequency is for phase images 13.86 mm, but this length has no influence in this case as the crack is on the surface of the sample. The penetration depth, which depends on the induction frequency, is in this case equal to 400 kHz, in order to increase heating of the material.

Penetration depth δ_s (mm)	Induction angular frequency (ω)	Induction frequency (f) (Hz)	Conductivity (κ) (S/m)	Permeability μ_0 (H/m)	Relative permeability
0,035	2513272	400000	1000000	1,25664E-06	500

Table 12: Penetration depth for a induction frequency of 400 kHz

As the induction frequency is very high, the eddy current penetration depth is very low. The induction frequency is now generated by a signal generator and can be changed easier than in the other setup.

The obtained results in this measurement have a good homogeneity due to the homogeneity of the magnetic fields and the defect is perfectly seen as in the other measurements. The boundaries of the crack are perfectly defined but the holes are not seen as well as in previous measurements.

7.4 Comparison of results: audio amplifier setup vs. old setup

The same sample was tested with the two induction thermography setups to compare the results.

Lockin frequency 1 Hz **Lockin frequency 0.1 Hz**

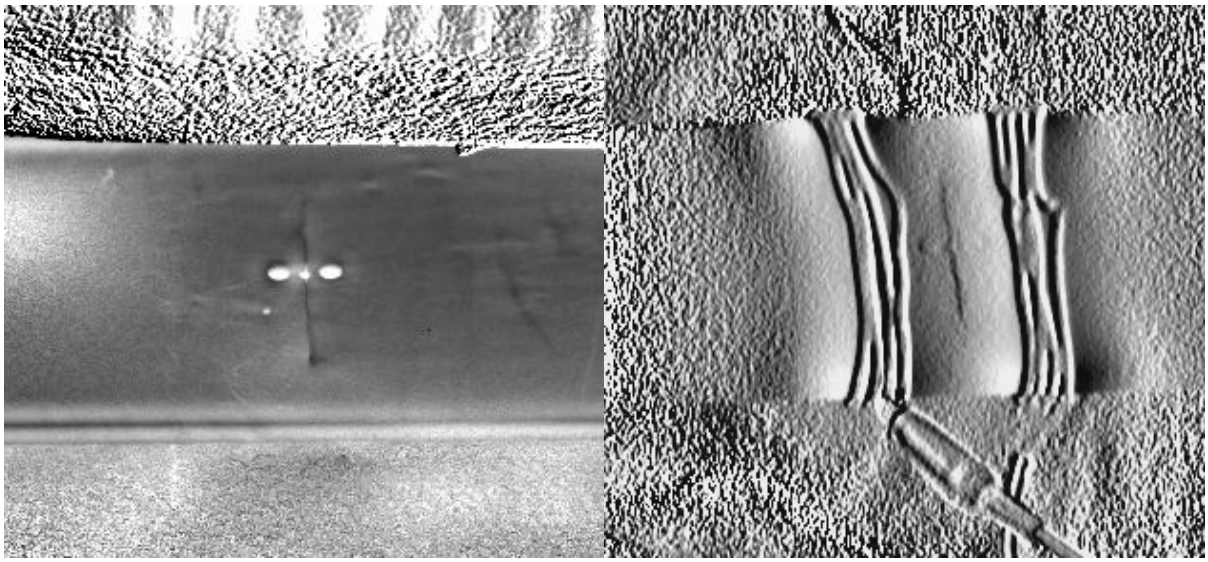

Figure 30: left, old setup, right new setup

The left image shows the result in the old setup with a cylindrical coil, which provides a good homogeneity. The defect is clearly seen.
The right image shows the measurement with the induction thermography setup with audio amplifier. The used inductor is a kind of a Helmholtz coil (section 7.2). The result in this case is very good and the boundaries of the crack are perfectly seen. It is also visible that only inside and near the induction coil a heating up appears – the image has defect selective properties as the surface crack has a much bigger signal than the intact material.
In the image of the induction thermography setup with audio amplifier, the Helmholtz coil have a radius of 20 mm and 4 windings per coil and in the first image, the radius of the cylindrical coil is 40 mm and the number of windings is 13, consequently, the magnetic field is higher in the first image and also the homogeneity, so the obtained result provides a better homogeneity and a better signal-to-noise.

8. Results and discussion

The results of the new cylindrical coil are compared with results obtained with a flat coil and also with results of OLT. Several parameters are compared, like the penetration of waves into the sample and the homogeneity of the magnetic fields. The results obtained with the Induction-Lockin-Thermography setup with audio amplifier are also compared with the results of the other setup.

8.1 Comparison of OLT with ILT

Several measurements on the same sample with different methods of lockin thermography and with different lockin frequencies were done for comparison.
To compare OLT with ILT and to see the differences between them, the measurements in metals must be done at the same frequencies in order to have the same penetration of the thermal waves into the material.

The results in both methods are very similar due to the skin effect at the induction heating of metals. With that the eddy current penetration depth has only few influence on the total depth range for defect detection. That is why the depth range for both methods are nearly the same.

8.2 Influence of inductor shape on results

A metal sample was used to compare the influence of the coil shape on the results in Induction-Lockin-Thermography. A flat coil and a cylindrical coil are used for the measurement.

The results show that the homogeneity is higher with the cylindrical coil than with the flat coil. The flat coil has a blind spot in the middle of the measurement area which is due to a lack of heating.
The outer field of the cylindrical coil is lower than the one of the flat coil – with that the signal-to-noise ratio of the results with the flat coil – outside the blind spot – are better than with the cylindrical coil.

8.3 New induction heating setup with audio amplifier

The cheap and easy induction heating setup with audio amplifier showed some very promising first results. A drawback of the setup is its low induced eddy current energy – with that the coil has to be wound around the sample under inspection in order to obtain a sufficient temperature modulation.

9. Conclusions

Induction-Lockin-Thermography is tested with different inductors to see the differences in the depth range and quality of resulting images for defect detection.
The cylindrical coil offers a higher homogeneity in the zones near the inductor compared to the induced heat of a flat coil. The drawback of the cylindrical coil – if the homogenous outer field is used – is its low magnetic field energy compared to the stronger field of the flat coil. In some degree this lower magnetic field can be compensated by a higher excitation amplitude.

Induction-Lockin-Thermography does not have a significant difference in depth range for defect detection in metals as compared with OLT. This is due to the skin effect which only improves the depth range for defect detection by the eddy current penetration depth which is several micrometers. The advantage of ILT over OLT is that it is not necessary to blacken the surface in order to increase the deposited heat.

In materials with lower electrical conductivity the eddy current penetration depth is much higher – but in CFRP it is limited again by electrical shielding of the carbon fibre layers. This is why also the results of OLT and ILT on CFRP are very similar.

At CFRP samples the orientation of the carbon fibres with regard to the magnetic field lines plays an important role. Only if the defect is parallel to the direction of the magnetic fields generated by the inductor, the defect is clearly seen and their boundaries are perfectly defined. When the defect is perpendicular to the direction of the magnetic fields, the defect is slightly seen and the boundaries are confused with the fibres, which compose the material.

The measurements on the metal sample with a surface crack show that Induction-Lockin-Thermography is a very good method for detection of such defects. In this

case the method even shows defect selective properties as the cracks are heated up higher than the intact material. So in this case the same advantage as in Ultrasound-Lockin-Thermography is obtained but with a non-contact excitation.

The new induction heating setup with audio amplifier also proved to be a good method to detect surface cracks in metal samples. This setup is still not very well developed, but the first tests with a Helmholtz like coil showed promising results. The drawback of this new setup is the relative low induced energy in the sample so that the higher inner field of the coil has to be used for sample excitation. This means that the coil has to be wound around the sample under inspection.

10. References

[1] D. Wu, A. Salerno, U. Malter, R. Aoki, R. Kochendörfer, P.K. Kächele, K. Woithe, K. Pfister, G. Busse, “Inspection of aircraft structural components using lockin thermography”. In: G. Busse, D. Balagueas, G.M. Carlomagno (Hrsg.):”Quantitative infrared thermography QIRT “96, 251-256, 02.-05.09.1996, Stuttgart.

[2] Xavier Maldague, “Nondestructive evaluation of materials by infrared thermography”, London , Springen Verlag, 224 p., 1993”, (new revised edition, John Wiley and Sons Pub., exp. In 2001).

[3] Spicer J.W.M., Kerns W.D., Aamodt L.C., Murphy J.C., “Time-resolved infrared radiometry (TRIR) of multiplayer organic coating using surface and subsurface heating” in Thermosense XIII, Proc. SPIE, G. S. Baird ed., 1467: 311-321, 1991.

[4] G. Busse, “Nondestructive evaluation of polymer materials”, NDT and E Int’l, 27 [5]: 253-262, 1994

[5] G. Busse, D. Wu, W. Karpen, “Thermal wave imaging with phase sensitive modulated thermography” , J. Appl. Phys., 71 [8]: 3962-3965, 1992

[6] Wu, D.; Salermo, A.; Rantala, J.; Busse, G. (1996), “Characterization of layered materials using lock-in thermography. 9th Internacional conference of Photoacoustic and Photothermal phenomena, Nanjing, China. Progress in natural science, supplement to Vol. 6 S.76-79.

[7] Rosenwaig, A.: Photoacoustic microscopy. In: American Lab 11 (1979) pp. 39-49.

[8] A. Dillenz, Th. Zweschper, G. Busse (2001), “Progress in ultrasound phase thermography” In: Proceedings thermosense, Orlando, FI (USA).

[9] Riegert, G.; Zweschper, Th.; Busse, G.: Lockin Thermography with Eddy Current Excitation. In: QIRT Journal. Volume I – n° 1/2004, Cachan Cedex: Lavoisier, pp. 21 – 31, ISBN: 2-7430-0725-7

[10] V. G. Welsby. - London : Macdonald, 1960. “The theory and design of inductance coils”

[11] Solenoids as magnetic field sources. http://hyperphysics.phy-astr.gsu.edu/hbase/magnetic/solenoid.html